CHALMERS
UNIVERSITY OF TECHNOLOGY

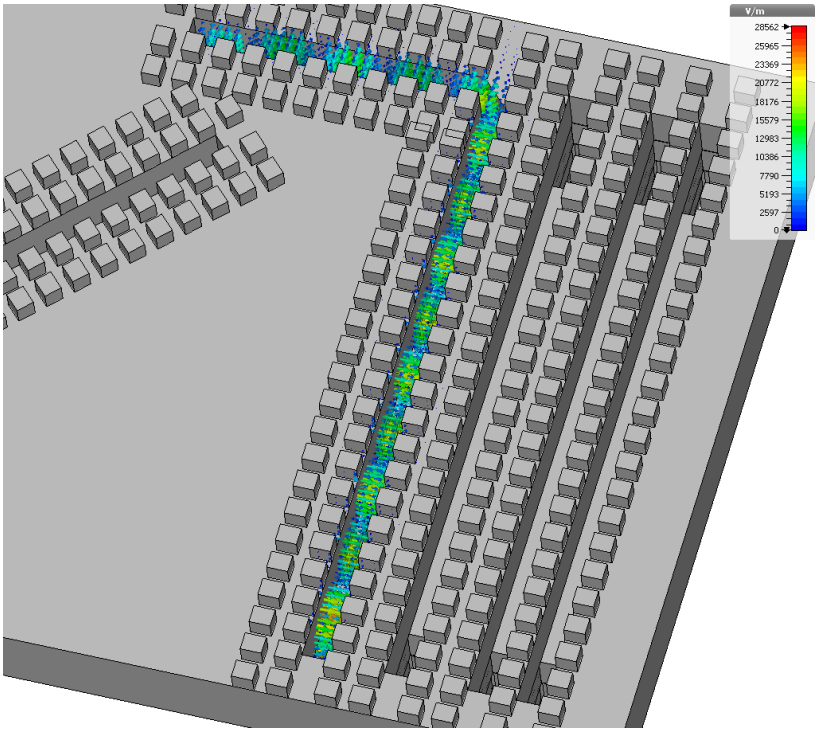

Design of Gap Waveguide Antenna System for 77 GHz Automotive Radar

A Study in the Implementation of Gap Waveguide Technology in Automotive Radars

Master's thesis in Wireless, Photonics and Space Engineering

HANNA KARLSSON

Department of Electrical Engineering
CHALMERS UNIVERSITY OF TECHNOLOGY
Gothenburg, Sweden 2018

Master's thesis 2018:NN

Design of Gap Waveguide Antenna System for 77 GHz Automotive Radar

A Study in the Implementation of Gap Waveguide Technology in Automotive Radars

HANNA KARLSSON

CHALMERS
UNIVERSITY OF TECHNOLOGY

Department of Electrical Engineering
Division of Communication and Antenna Systems
Antenna Systems Group
Chalmers University of Technology
Gothenburg, Sweden 2018

Design of Gap Waveguide Antenna System for 77 GHz Automotive Radar
A Study in the Implementation of Gap Waveguide Technology in Automotive Radars
HANNA KARLSSON

© HANNA KARLSSON, 2018.

Supervisor: Assistant Professor Ashraf Uz Zaman, Department of Electrical Engineerng, Chalmers
Supervisor: Abolfazl Haddadi, Gapwaves Examiner: Professor Jian Yang, Department of Electrical Engineerng, Chalmers

Master's Thesis 2018:NN
Department of Electrical Engineering
Division of Communication and Antenna Systems
Antenna Systems Group
Chalmers University of Technology
SE-412 96 Gothenburg
Telephone +46 31 772 1000

Cover: E-field propagation inside a Gap Waveguide routing structure.

Typeset in LaTeX
Printed by [Name of printing company]
Gothenburg, Sweden 2018

Design of Gap Waveguide Antenna System for 77 GHz Automotive Radar
A Study in the Implementation of Gap Waveguide Technology in Automotive Radars
HANNA KARLSSON
Department of Electrical Engineering
Chalmers University of Technology

Abstract

The automotive industry is evolving quickly towards self-driving cars, with automated technology becoming more common with every new model. In order for full automation to become reality, there is a need for high-performance radar systems which manages to meet the standards while keeping a low cost. This thesis work presents a study in gap waveguide technology and its possible advantages in the automotive radar industry at 76-77 GHz compared to current microstrip-based solutions. The methodology includes both literature study and extensive simulations using the electromagnetic solver CST, and the thesis work was divided into two parts. The first part concerned existing automotive antennas, and how to design a 8-slot single column antenna for automotive purposes. This column was compared to existing solutions and to reference simulations on a microstrip antenna. The first part of the thesis work also included a tolerance analysis of a microstrip-to-double ridge waveguide, since this can be an essential part of an automotive radar system. The second part of the thesis work involved routing from waveguide ports using gap wavwguide technology, and examined how this could be implemented and which problems it faced.
The results show that the gap waveguide antenna can compete with current microstrip-based solutions, but that there is still further work to be done concerning more advanced gap waveguide routing systems. Potential future applications involve frequency extention to 77-81 GHz for the antenna, and incresing the robustness of the gap waveguide routing.

Keywords: Automotive, Gap Waveguide, Radar, Slot Antenna, W-band.

Acknowledgements

This thesis work was carried out at Chalmers University of Technology in close collaboration with Gapwaves AB.
I would like to thank my supervisors, assistant professor Ashraf Uz Zaman at Chalmers and Abolfazl Haddadi at Gapwaves for guiding me through my thesis work with your knowledge. I also would like to thank professor Jian Yang, examiner, and adjunct professor Thomas Emanuelsson, CTO at Gapwaves, for good input during meetings.
A big thanks to everyone at Gapwaves for making me feel welcome in your office and helping me whenever I needed. I also wish to give a well-deserved thank you to the coffee machines both at Chalmers and Gapwaves, for always being there for me in desperate times and always supporting me.
To my family and friends whom have supported me all through my education; I do not know how you managed to tolerate me and I will be forever grateful for all you have done.

Hanna Karlsson, Gothenburg, June 2018.

Contents

List of Figures

List of Tables

1
Introduction

This thesis work involves six chapters in the following order; Introduction, Theory, Method, Results, Discussion and Conclusion.

1.1 Background

Cars are an essential part of many peoples everyday life and is needed for every type of trip, ranging from shorter distances in urban areas to long drives through continents. In 2017, the total distance driven by individuals owning cars in Sweden amounted to nearly 50 billion kilometers, which is on average 12 000 km per car owning person [1]. But commuting to work every day is something many people dread, since the time spent driving through the morning traffic stock could be used for something else. One of the possible solutions to this problem would be to not drive at all, but instead let the car do the driving.
The research about autonomous driving can not be considered modern since it have been ongoing for several decades, with both commercial and academic developers such as the Carnegie Mellon University development program Navlab or Mercedes-Benz participation in the Prometheus-project [2],[3]. Even though the driver assistance systems keeps getting more and more sophisticated, there is not yet a fully autonomous car available commercially.
The Society of Automotive Engineers, or SAE, have defined six steps of car automation that is generally agreed upon. These six steps are divided into two subsections, where in the first three levels the driver performes part or all of the dynamic driving tasks and in levels 3-5 the automated driving system does this instead. These levels are described in Figure 1.1.
All autonomous vehicles, independent on SAE-level, relies heavily on the functionality of its sensors. There are several different sensors in a modern car today, such as LIDAR utilizing lasers or GPS-receivers which keeps track of the position of the car.

1.1.1 Automotive Radars

For many years the 24 GHz-band was utilized for automotive radars, but recently the industry has moved towards the W-band at 76-81 GHz. Even though radars at 24 GHz are easier to engineer due to its longer wavelength, the higher-frequency band makes it possible to have smaller systems with higher performance. This allows for longer range radars which takes up less space in the generally crowded bumper

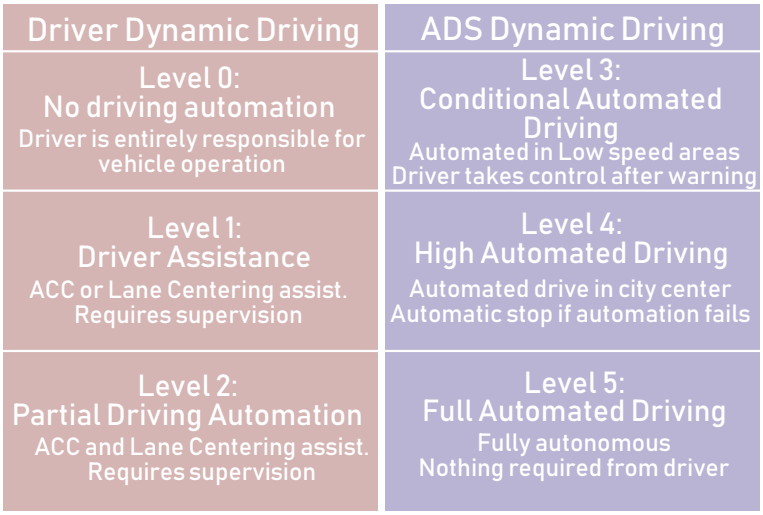

Figure 1.1: Levels of automation as determined by SAE.

of the car. A comparison of using the 24 GHz-band versus using the 77 GHz-band are given in Table 1.1.

Table 1.1: Comparison between 24 GHz and 77 GHz [5].

24 GHz	**77 GHz**
Easier to engineer	Difficult in engineering point-of-view
Generally lower performance	Higher performance sensors are possible
Approx. 3 times larger antenna aperture compared to 77 GHz	Small antenna size → small sensor size
Lower angular resolution when using same aperture size (see Equation 2.13)	Higher angular resolution when using same aperture size (see Equation 2.13)
Combination of high transmit power and high bandwidth not allowed	High transmit power and high bandwidth allowed → Long range and high distance separability
Cheaper products compared to 77 GHz when using same method	More expensive product, but smaller sensors → less packaging costs
Longer wavelength → behind-bumper-integration easier since thickness of bumper doesn't influence as much	Behind-bumper-integration more challenging due to much shorter wavelength and bumper thickness in the same magnitude

The safety systems of a car is divided into two main categories: **passive** and **active** control. An example of passive control is airbag inflation after a crash, and this occurs after a certain specific scenario have taken place. Passive control also may

require the driver to take action, such as warnings of a slippery road urging the driver to be careful and perhaps drive slower. The active control systems can control mechanisms of the car like brakes, steering etc. where adaptive cruise control (ACC) is an example of such a system. The ACC is a system that will adjust the speed of the car depending on traffic ahead, and thus takes control of the gas and/or the brakes of the car [5].
The ACC is an example of a system utilizing long-range radar, which is set to operate 100 m ahead and beyond. The mid-range radar generally operates in a region of 40-100 m, and the short-range radar operates below 40 m even though these limits are a bit floating [6]. A function of a mid-range radar is for example the lane-change assistant, which checks the blind spot for the driver when changing lanes for overtaking or in multiple-lane environments. Short-range radar applications includes parking aids and cross-traffic alerts, which warns the driver when there are objects approaching in a junction or when driving out from a parking lot [5].
The radar consists of two main parts: the radar chip and the antenna. The chip is a PCB which contains the transceiver with all parts necessary for generating and receiving the signal. The radar antenna consists of both transmit (Tx) and receive (Rx) antennas, generally with more than one element each. The antennas can be created in many different ways, ranging from lens antennas with a patch feed or slot arrays. Some of the requirements on an automotive antenna include:

- The antenna should be appropriate for mass production.
- The antenna should be able to handle large temperature shifts, generally from -40° up to +85°.
- It is necessary for the antenna to perform well in harsh environments, with large vibrations and shocks.
- A small size of the finished product is crucial for the possibility to integrate the antenna into the car properly. In general, it is the antenna that sets the size of the whole radar system [6].

1.1.2 Gap Waveguide Automotive Radars

A transceiver used for automotive radar purposes which utilizes gap waveguide technology may be divided into four parts. These parts include:

1. The PCB-chip with possible microstrip routing to waveguide ports. This part will not contain any gap waveguide-structures.
2. Gap-waveguide routing from waveguide ports to antenna ports. This may not be necessary if the routing is already done using microstrip.
3. Transition from microstrip to waveguide port. This normally consists of both metal pins above the microstrip transmission lines and mushrooms in the PCB substrate.
4. The antenna array, with either a groove gap waveguide or ridge waveguide where each antenna column is surrounded by metal pins.

1.2 This Work

The purpose of this master thesis project is to study the use of Gap Waveguide-structures when implemented in automotive radar concepts, to describe its advantages and drawbacks and compare it to existing solutions which uses other types of structures such as microstrip. This examination includes all parts from the PCB to the antenna; the gap waveguide routing, the transition and the antenna element itself.
The aim of the study is to investigate the advantages and drawbacks of gap waveguide structures in an automotive environment, and to determine its stand compared to conventional radar system methods.
There are several aspects of a gap waveguide-based radar system that could be examined, but for the sake of the thesis this needs to be restricted. The master thesis work will focus on the routing, transition and antenna, deciding which parameters governs the performance. No focus will be put on the radar chip itself, since it will not include any gap waveguide-related parts. It is also important to note that the requirements on the automotive radar performance highly depends on the desired functionality, i.e. if the radar is supposed to work long or short range and if it is to be used for imaging (SAR) or more traditional monostatic applications. It is not in the scope of this master thesis work to examine all different applications of automotive radar. The thesis work will be divided into two parts: Part 1: Gap Waveguide Automotive Radar Antenna and Transition and Part 2: Advanced Radar systems.

1.2.1 Part 1: Gap Waveguide Automotive Radar Antenna and Transition

How will Gap Waveguide designs improve the performance compared to existing PCB-based solutions? Part 1 will cover two main topics: **Antenna Design** and **Transition tolerance analysis**. The antenna design will involve optimizing a single element ridge waveguide antenna with and without transition to microstrip, and to create an antenna array consisting of 3 Tx and 3 Rx-channels. The transition tolerance analysis will focus on which parameters that plays an important role in the transition design, and which properties each part holds.

1.2.2 Part 2: Advanced Radar Solutions

Some automotive radar systems require more advanced structures, especially if the system is to be used for imaging. These type of radars will have more Rx- and Tx-channels compared to conventional radar systems, and thus need more complex routing. In part 2 of the thesis work, such an advanced routing system will be constructed using gap waveguide technology. The governing parameters for routing will first be determined in hollow waveguide, for it to be translated to include gap waveguides.

2
Theory

The theory chapter includes both antenna, gap waveguide and radar basic concepts. In Section 2.1 basic concepts about scattering parameters and hollow waveguides are explained, as well as specifics about slot antennas. In Section 2.2 the problems with using hollow waveguides in routing systems are discussed and simulation results are presented. Gap waveguide technology is described in Section 2.3, followed by some basic radar concepts in Section 2.4.

2.1 Antenna Theory

This section includes basic microwave theory about scattering parameters, general characterization parameters used in antenna design and waveguide slot antenna theory.

2.1.1 Scattering parameters

Scattering parameters, more widely known as S-parameters, are used to determine the performance of a microwave system with N ports. The S-parameters relates the voltage incident on a port to the reflected voltage, and can describe system characteristics such as input matching or port-to-port loss. For an N-port network, the S-parameter matrix is defined as

$$\begin{bmatrix} V_1^- \\ V_2^- \\ \vdots \\ V_N^- \end{bmatrix} = \begin{bmatrix} S_{11} & S_{12} & \dots & S_{1N} \\ S_{21} & \ddots & & \vdots \\ \vdots & \dots & & \\ S_{N1} & \dots & & S_{NN} \end{bmatrix} \begin{bmatrix} V_1^+ \\ V_2^+ \\ \vdots \\ V_N^+ \end{bmatrix} \tag{2.1}$$

where V_N^- corresponds to the reflected voltage amplitude and V_N^+ is the incident voltage amplitude. The S-parameters can be calculated from

$$S_{ij} = \left. \frac{V_i^-}{V_j^+} \right|_{V_k^+=0} \tag{2.2}$$

where $V_k^+ = 0$ holds for $k \neq j$ and means that all other ports than i,j are terminated in matched loads. For instance, S_{11} is then the reflection coefficient at port 1 if all other ports would be terminated in a matched load [7].

2.1.2 General Antenna Characterization Parameters

There are several parameters that determines the performance of an antenna, ranging from side lobe level (SLL) to gain or directivity to co- and cross-polarization level. Depending on application, these characteristics matter to different extents. In automotive radar antennas, there are a couple of parameters that needs to be examined in order to properly evaluate the antenna performance.

Power Gain. The power gain G of an antenna is defined as the radiation intensity in a given direction compared to the radiation intensity of an uniformly radiating antenna with the same input power. This is calculated as

$$G = \frac{4\pi U(\theta, \varphi)}{P_T} \tag{2.3}$$

where $U(\theta, \varphi)$ is the radiation intensity in a given direction and P_T is the total power delivered to the antenna port.

Directive Gain. The directive gain D represents the radiation intensity in a given direction compared to the total radiated power, and is expressed as

$$D = \frac{4\pi U(\theta, \varphi)}{P_R} \tag{2.4}$$

where P_R is the total radiated power.

Directivity. One of the key parameters when discussing antenna performance is the directivity D_0, which is derived from the directive gain of the antenna. It is defined as the value of directive gain in the center of the main beam, so for beams centered at zero it is given as

$$D_0 = \frac{4\pi U(0, 0)}{P_R} \tag{2.5}$$

The relationship between gain and directivity is related to the antenna efficiency, and the gain in the center of the main beam G_0 can be calculated as

$$G_0 = e_{\text{rad}} e_{\text{pol}} D_0 \tag{2.6}$$

where e_{rad} is the total radiation efficiency and e_{pol} is the polarization efficiency of the antenna [9].

2.1.3 Waveguide Slot Array Antennas

A waveguide slot antenna is a waveguide, rectangular or circular, with one or several radiating slots on the waveguide walls. Usually the waveguide is air-filled, but it is not uncommon with models containing a dielectric in order to reduce the guided wavelength. Due to low loss and the possibility for high power, waveguide slot antennas are widely used for microwave frequency applications such as communication

systems or radars [8]. A waveguide-fed slot antenna is also easily made into an antenna array, which in turn can be put side-by-side in order to create even larger two-dimensional arrays [9].

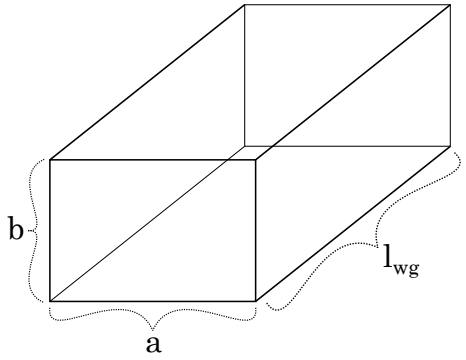

Figure 2.1: A basic waveguide layout, indicating the width (a), height (b) and length (l_{wg}).

The work of theorizing the slot fields in rectangular waveguides was performed by Stevenson in 1947, and is still used today in waveguide slot antenna designs. In Figure 2.2 the different design parameters taken into consideration is shown. The general assumptions used for design of a slot antenna are that the waveguide walls are very thin and perfectly conducting, and that the width of the radiating slot is much smaller than the length. A general rule for the relationship between the slot width w and length l can be written as

$$2\log\left(\frac{l}{w}\right) \gg 1 \tag{2.7}$$

In general, the length of the slot is designed to be half a wavelength $\lambda_g/2$ [10], where λ_g is the guided wavelength determined by the propagation constant β (or the rectangular waveguide broad dimension a as given in Figure 2.1) as

$$\lambda_g = \frac{2\pi}{\beta} = \frac{\lambda_0}{\sqrt{1-\left(\frac{\lambda_0}{2a}\right)}} \tag{2.8}$$

with λ_0 corresponding to the free-space wavelength. The slot separation $\mathrm{d_{slots}}$ are set to approximately half a guided wavelength. The slot offset from the centerline $\mathrm{d_{offset}}$ of the broad waveguide wall will affect the excitation strength of the slot, i.e. if the slot is positioned closer to the centerline the excitation strength will be larger.

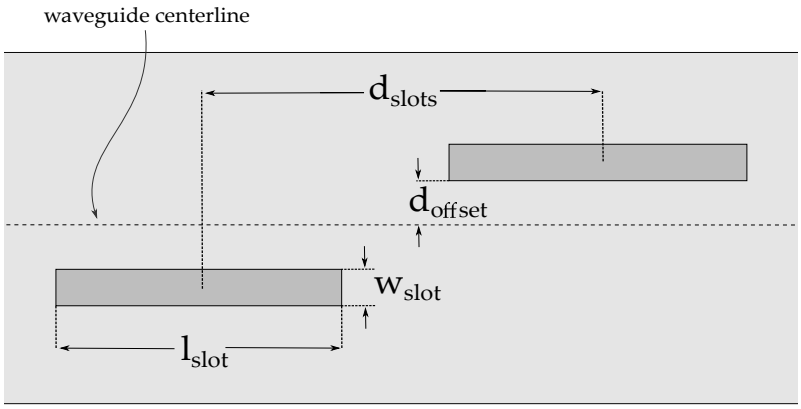

Figure 2.2: Schematic showing the primary slot parameters on a waveguide slot array antenna, with the slots located on the broadside of the waveguide. The centerline is indicated and is positioned at a distance of $a/2$. The separation between neighbouring slots d_{slots} is measured from the center of each slot.

There are considered to be three main type of antenna arrays; Resonant array, Travelling wave array and Leaky Wave array. For a resonant array, the antenna waveguide is designed with a length that will form a standing wave-pattern inside the antenna which means that the end of the antenna is short-circuited. This gives the resonant array antenna a broadside beam, but it usually needs some further input matching. In a travelling wave array a matched load is positioned at the end of the antenna avoiding a standing wave, and this gives it an advantageous input return loss. For the leaky wave array, a matched load is used and the antenna elements forms a periodic perturbation along the transmission line which will not result in a broadside beam [9],[11].

2.2 Hollow Waveguide Limitations

Hollow waveguides are generally praised for their low loss for millimeter wave applications, but in manufacturing they may be problematic. Normally the waveguides are produced in two pieces, either by E-plane cut or H-plane cut, and then assembled together. This method would be good if it were flawless, but unfortunately there may occur misalignments and air gaps between the two pieces resulting in reduced performance [27]. In the following sections, simulation results for hollow waveguides with misalignments and coupling between transmission lines will be presented.

2.2.1 H-plane cut

If the waveguide is cut in the same direction as the broad wall a, it is parallel with the magnetic field lines of the first mode and is thus referred to as a H-plane cut. This cut is shown in Figure 2.3.

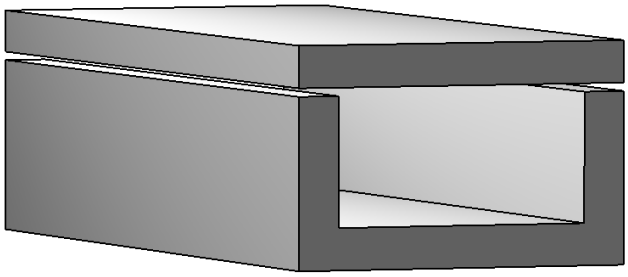

Figure 2.3: Hollow waveguide structure with H-plane-cut

In Figure 2.4, two H-plane cut transmission lines are shown with parameters `air_gap` and `wg_separation` indicated. Since the top piece of the H-plane cut is flat, there is no misalignments to regard in this case.

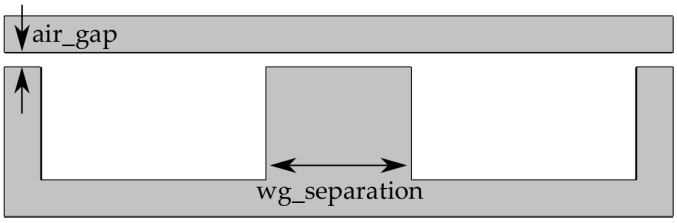

Figure 2.4: Hollow waveguide structure with H-plane cut, as seen from the front with the parameters `air_gap` and `wg_separation` indicated.

The H-plane cut performance is shown in Figures 2.5a-2.6b, where simulation results are presented for different air gaps. Figure 2.5a shows the return loss, Figure 2.5b shows the transmission coefficient, Figure 2.6a displays the adjacent port coupling and Figure 2.6b shows the opposite port coupling. As can be seen in the figures, the air gap starts to influence the performance after 30 μm and above, whereas 20 μm behaves almost as an ideal waveguide.

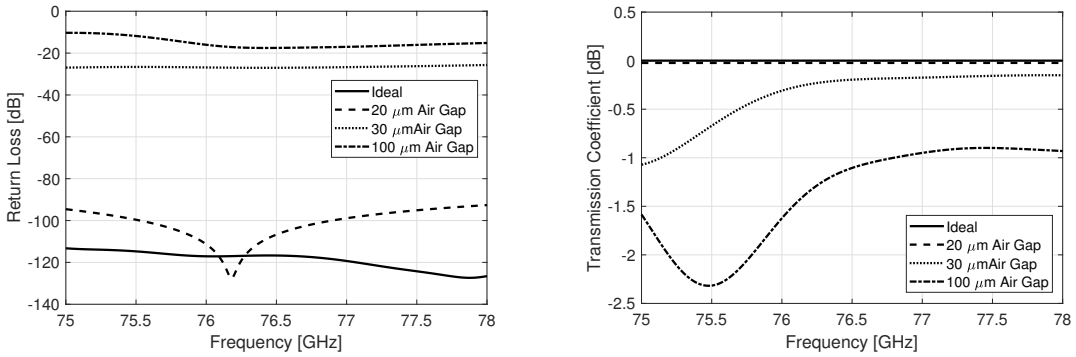

(a) Return Loss **(b)** Transmission Coefficient

Figure 2.5: Return loss (a) and Transmission Coefficient (b) for H-plane cut hollow waveguide with different air gaps.

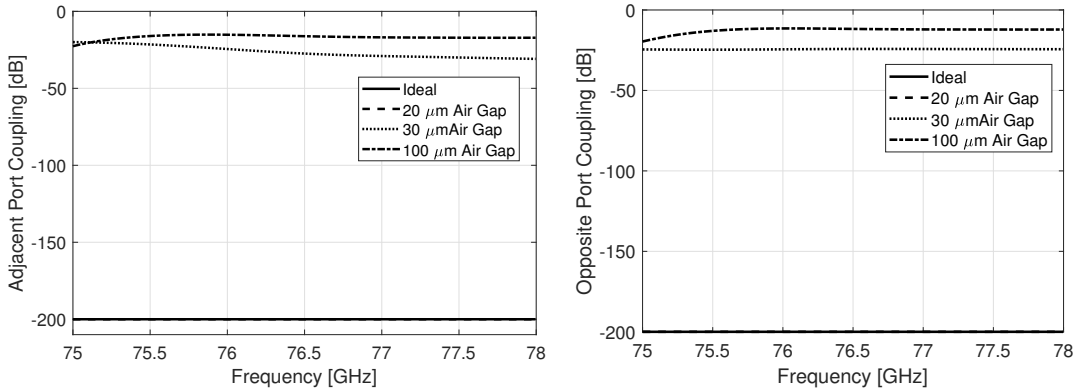

(a) Adjacent Port Coupling **(b)** Opposite Port Coupling

Figure 2.6: Adjacent Port Coupling (a) and Opposite Port Coupling (b) for H-plane cut hollow waveguide with different air gaps.

2.2.2 E-plane cut

The E-plane cut is parallel to the E-field lines for the fundamental HWG-mode, and is shown in Figure 2.7 where the waveguide is placed on the short wall facing down. This type of cut can, except to air gaps, be subject to misalignments between the top and bottom pieces. This is shown in Figures 2.8a-2.8b.

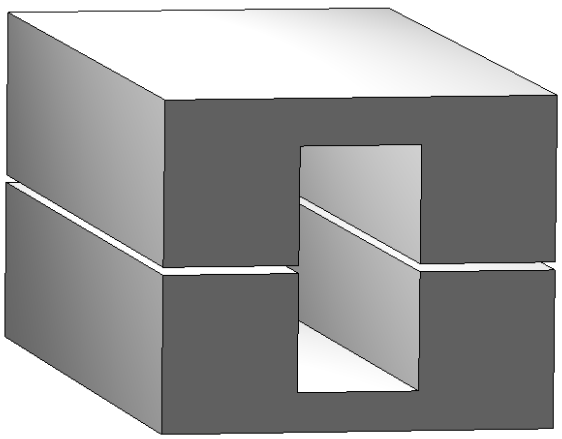

Figure 2.7: Hollow waveguide structure with E-plane-cut, flipped on its short edge.

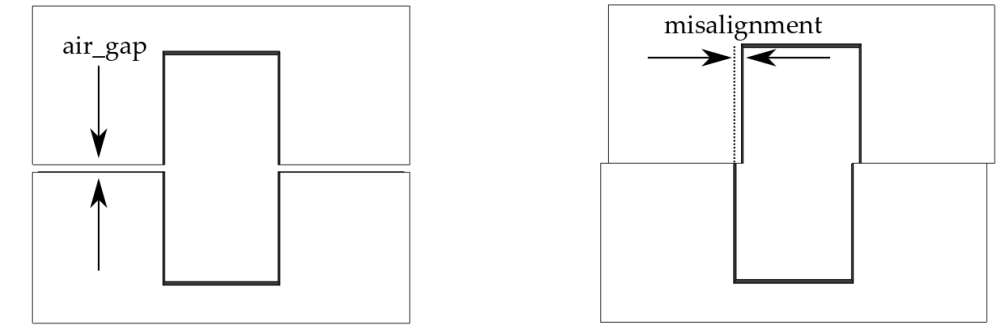

(a) Air Gap **(b)** Misalignment

Figure 2.8: E-plane cut hollow waveguide structure with exaggerated (a) air gap and (b) misalignment.

The E-plane cut hollow waveguide performance is shown for different air gaps in Figures 2.9a-2.10b and for misalignments in Figures 2.11a-2.11b. It can be seen that for air gaps of 0.2 mm the performance is affected but an air gap of 0.1 mm does not influecne the performance significantly. The coupling remains low for all air gaps, for both the opposite and adjacent ports. It is also seen that a misalignment of 0.1 mm will affect the result, but the waveguide performance is still good. Introducing an air gap along with misalignment reduces the performance further.

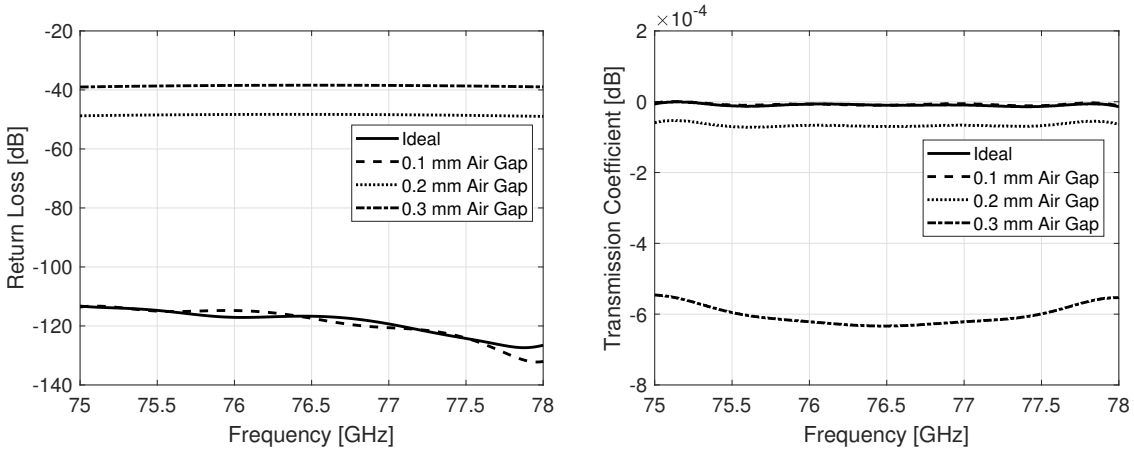

(a) Return Loss **(b)** Transmission Coefficient

Figure 2.9: Return Loss (a) and Transmission Coefficient (b) for E-plane cut hollow waveguide with different air gaps.

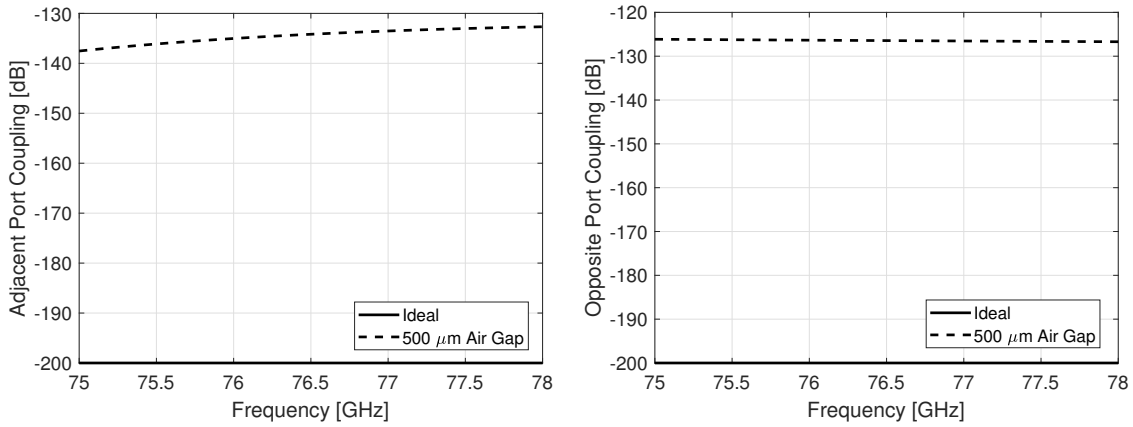

(a) Adjacent Port Coupling **(b)** Opposite Port Coupling

Figure 2.10: Adjacent Port Coupling (a) and Opposite Port Coupling (b) for E-plane cut hollow waveguide with different air gaps.

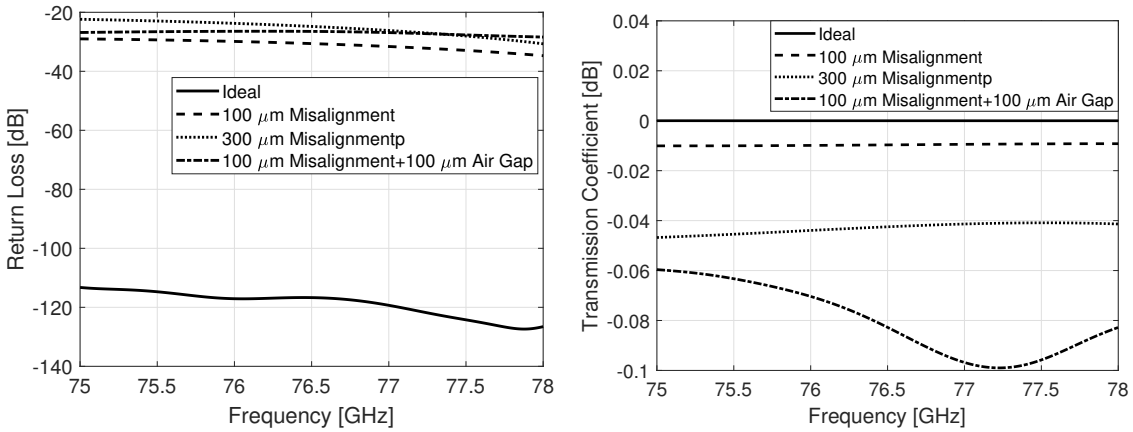

(a) Return Loss **(b)** Transmission Coefficient

Figure 2.11: Return Loss (a) and Transmission Coefficient (b) for E-plane cut hollow waveguide with different misalignments and air gap.

2.3 Gap Waveguide-technology

The theory section covering gap waveguide technology begins with presenting the idea about soft and hard surfaces, followed by describing the three types of gap waveguides used in this thesis work.

2.3.1 Soft and Hard Surfaces

The Gap Waveguide-technology is an application resulting from the research about soft and hard surfaces presented by Per-Simon Kildal in 1988. The terminology for a surface to be "soft" or "hard" originates from acoustics, where a soft surface is a

surface where the density of the power flow is zero along the surface. This is the same for a soft electromagnetic surface, where the Poynting vector along the surface is zero independent of polarization. Reciprocally, a hard surface is a surface where the Poynting vector of the electromagnetic wave exhibits a maximum. The hard surfaces can be achieved by for instance longitudinal corrugations on the surface, and soft surfaces is thus possible to realize by transverse corrugations [19]. This method of creating hard surfaces can be utilized to allow for quasi-TEM wave propagations in rectangular waveguides, since the hard surface can suppress any propagation but the quasi-TEM-mode when used with a guiding structure. This is due to the transverse propagation being suppressed while propagation in the axial direction is favoured, creating the quasi-TEM-mode desired [26].
The hard surface behaves as an artificial magnetic conductor (AMC), and the frequency range of which the surface prohibits propagation is reffered to as stopband. For a parallel plate waveguide there are other ways of realizing a stopband apart from corrugations, such as metal patches with vias ("mushrooms") incorporated into the substrate or a bed of nails [21]. The Gap Waveguide-technology relies on creating a bed of rectangular nails, with either a groove or ridge as guiding structure for the field.

2.3.2 Types of Gap Waveguide Structures

There are different types of gap waveguide-structures such as ridges, bed of nails (pins) or mushrooms, all providing the desired AMC. The thesis work will mainly focus on beds of nails consisting of square metal pins, but will also cover in short PCB-based mushrooms.

2.3.2.1 Pin Structure

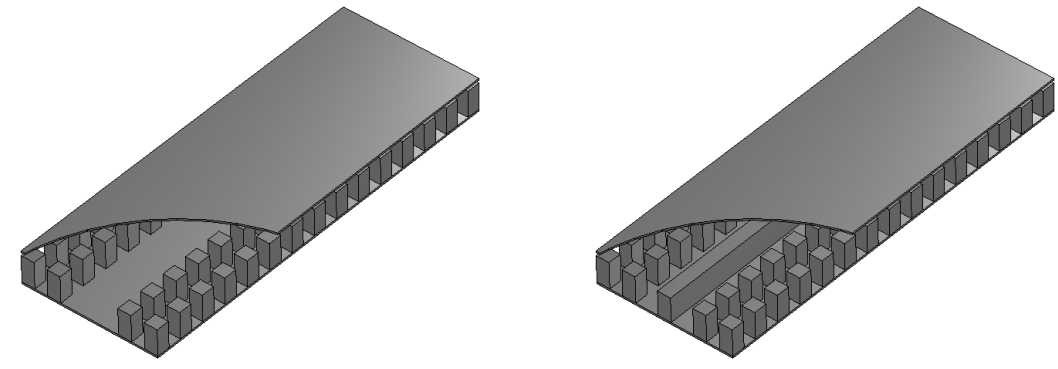

(a) Groove **(b)** Ridge

Figure 2.12: Examples of (a) Groove Gap Waveguide and (b) Ridge Gap Waveguide.

Two types of gap waveguide structures are shown in Figures 2.12a- 2.12b. The waveguide itself is either based on hollow wavegudie as in groove gap waveguides or using a guiding ridge as in ridge gap waveguides. The groove or ridge is then surrounded by one or more rows of pins where the pin size (height d and width w), period p and air gap h between pins and top (lid) are the parameters which determines the desired properties of the AMC-surface [27]. These parameters are shown in Figure 2.13.

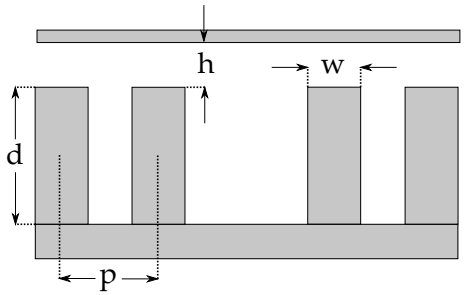

Figure 2.13: Configuration of pin structure (front view) with a groove gap waveguide.

For a constant pin size and period, the stopband of the AMC will be increased by a smaller air gap between pins and lid. In general the height of the pin is kept at a quarter wavelength, whereas the air gap h is desired to be smaller than $\lambda/4$. For periods larger than 0.25λ, there may occur propagation of higher order modes and thus the upper frequency limit of the stopband is reduced.

2.3.2.2 Mushroom Structure

An example of a mushroom-based AMC with a microstrip ridge as guding structure is shown in Figure 2.14a.

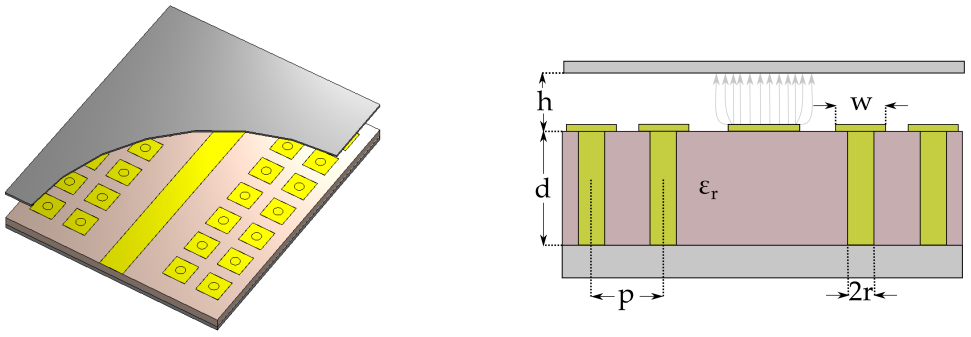

(a) Top View. **(b)** Front View.

Figure 2.14: Mushroom structure with guiding ridge: (a) top view, (b) front view where the different structure parameters are denoted.

The mushrooms consists of metal via holes with either circular or square microstrip patches, and these mushrooms are arranged into periodic structures in order to

create an AMC. As for the gap waveguide, it is desired to keep the air gap between the mushroom and the lid h smaller than $\lambda/4$. The radius r of the grounded pins will determine which position in the frequency spectrum the stopband have, where a larger radius results in a higher frequency. The separation between the mushroom patches i.e. $p-w$ seems to have the most effect when the air gap h is very small [20].

2.3.3 Gap Waveguide Packaging

For RF-components operating at mm-wave frequencies and above, conventional packaging techniques for reduction of inter-component coupling and for shielding are not as effective as for lower frequencies. Conventional techiques includes using for instance lossy absorbers, bond wires and/or metal walls to shield the components, but this may cause resonances and interference caused by the presence of the packaging itself. Instead, a gap waveguide-based packaging may be used for high frequency components [27]. For high frequnecy antenna array systems, the substrate losses may be large and bond wires needed for integration of MMIC-parts can act inductive. This is prevented by the use of gap waveguide structures in work by Zaman et.al, where pyramid-shaped pins are used for packaging at 60 GHz and above [22]. An AMC pin structure is also used in [23], where a solution for integrating MMIC microstrip components to waveguide is presented which removes the need of RF bond wires and small probe substrates.

2.3.4 Gap Waveguide Passive Structures

The gap waveguide-technology can be used for high frequency passive components such as couplers, filters and adapters since these are components that suffers from losses at high frequencies when designed in e.g microstrip structures. It is also possible to produce these components in waveguide technology, but for higher frequencies this introduces a higher manufacturing and assembly cost.
Alfonso et.al. presents several usages of passive gap waveguide structures in [24]. For instance, a Riblet hybrid coupler for 37-40 GHz was constructed where measurements showed good isolation while obtaining the desired 3 dB coupling. The same paper also presents a narrowband gap waveguide-based bandpass filter for 38 GHz applications.
For transcievers in automotive radars, there may be use for diplexers separating the Tx and Rx-signals while guiding them to their respective antenna ports. Such a diplexer was designed with groove gap waveguides in [25] for 60 GHz-applications.

2.3.5 Gap Waveguide Antennas

There exists today several published papers regarding the design and fabrication of gap waveguide slot antennas for different frequency bands. A groove gap waveguide-fed slot array at 37.5 GHz was constructed by Jimenez Saez et.al. in 2016 which have a feeding network similar to this thesis where the groove gap waveguide is placed with the short end facing down [28]. A ridge gap waveguide feeding network have been used by e.g. Zarifi et.al. in [29], where it is fed into a slot array antenna used for 60 GHz.

2.4 Basic Radar Concepts

A monostatic radar measurement relies on the principle of transmitting a signal and examining the reflection back to the receiver. One of the parameters characterizing a radar system is its ability to measure range, i.e. distance to objects and this is determined by measuring the time Δt it takes for the signal to return to the radar sensor. The range R of an object can be determined by

$$R = \frac{c\Delta t}{2} \tag{2.9}$$

where c is the speed of light and Δt is the time it takes between transmitting the signal and receiving it again. The factor 2 appears since the wave travels the full range distance twice.
The basic principle describing how a radar system works is shown in Figure 2.15. A signal is generated in the transmitter and transmitted. The signal will reach an object and be reflected, where the amount of reflection depends on the object property. The signal reaching the receiver is then compared (or mixed) with the transmitted signal. The received signal can then be further processed digitally, e.g when implementing digital beamforming.

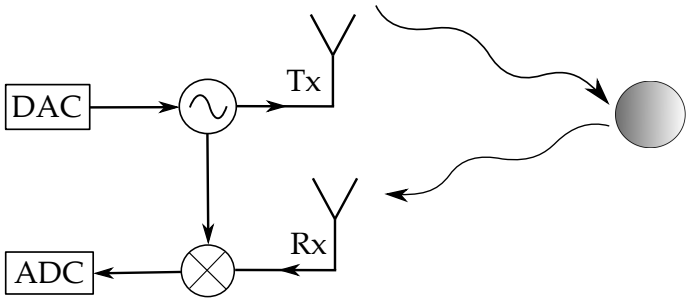

Figure 2.15: A simple schematic showing the basic principle of a radar system.

Automotive radar generally uses Frequency Modulated Continuous Wave (FMCW), which sends a signal where the frequency changes within one pulse. This is also referred to as a chirp signal. A plot showing a transmitted chirp-signal and the corresponding received signal is given in Figure 2.16.

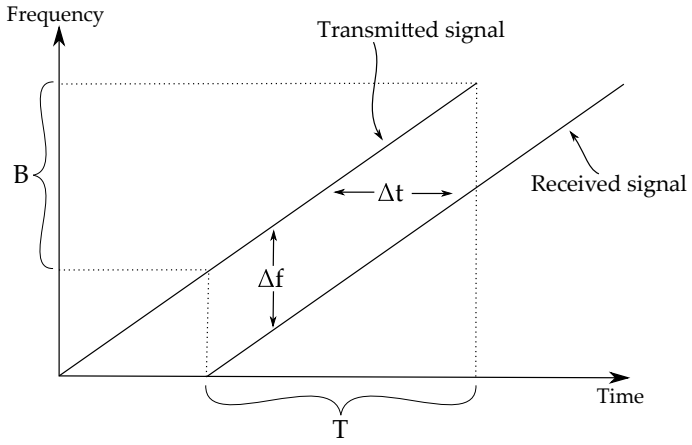

Figure 2.16: Frequency versus time for a transmitted chirp signal and the corresponding received signal.

In Figure 2.16, Δf is the frequency difference between the received and transmitted signal at a specific time t and B is the bandwidth of the chirp signal [12].

2.4.1 Range resolution

One of the main properties characterizing the performance of a radar system is the *range resolution* ΔR, which describes how close two objects can be and still be detected by the radar as separate targets. The range resolution relies heavily on the width of the mainlobe of the waveform, and this can be specified in two different ways. The first way is to determine the width of the mainlobe at a specific point below the peak value such as -3 dB or -6 dB, and use this as a figure of merit on how the radar is performing. This can be difficult to compare since the shape of the mainlobe may vary depending on e.g. modulation. Another approach is to use the Rayleigh criterion, which defines range resolution as when the peak of the matched filter response of the first object coincides with the first null of the second object. This is due to no or negligible energy from the first object interfering with the peak of the second objects return. When using pulsed radar with a pulse duration τ, the range resolution is given by

$$\Delta R = \frac{c\tau}{2} \tag{2.10}$$

This is true for when the pulse width and bandwidth are the inverse of one another. More generally it can be said that the resolution is proportional to the bandwidth of the waveform as

$$\Delta R = \frac{c}{2B} \tag{2.11}$$

where B is the waveform bandwidth. Equation 2.11 can be generalized to

$$\Delta R = \kappa \frac{c}{2B} \tag{2.12}$$

where κ is a scale factor for circumstances that will degrade the resolution [13].

2.4.2 Angular Resolution

The angular information about a target both in elevation and azimuth is determined by the angular resolution of the antenna system [5]. The angular resolution $\Delta\varphi$ is characterized by the Rayleigh criterion as

$$\Delta\varphi = 1.22\frac{\lambda}{d} \tag{2.13}$$

where λ is the wavelength and d is the aperture size in the desired orientation [14].

3
Methods

3.1 CST Microwave Studio

There are several electromagnetic simulation modules for high-frequency applications available today, such as HFSS or FEKO. In this thesis work the microwave studio of Computer Simulation Technology, or more commonly CST, have been used. CST Microwave studio is one of the most widely used tools for high-frequency simulation applications, and provides both time and frequency solvers [15].
The solver type depends on the simulation itself, where result accuracy and CPU-time are two components that needs to be weighed against one another. The transient solver utilizes the finite integration technique (FIT), which solves Maxwells integral equations using tetrahedral or hexahedral meshes [16]. This work almost exclusively used the transient solver, since it was regarded as quicker compared to the frequency solver but still with satisfying accuracy. In some cases however it was necessary to use the frequency solver instead, since the ports could not be aligned with one of the fundamental planes and this is necessary for the transient solver.
Optimization is a large part of the design process and allows for performance refinement after consulting textbooks and equations. In this work, the Genetic Algorithm have been the main algorithm used in optimization routines. This is because it optimizes on a global scale and is suitable for when one wishes to optimize a large number of structures. The Genetic algorithm works evolutionary, which means that it evaluates parameter sets and then choose to continue evaluating the most suitable ones through multiple generations until optimization is complete [17].
The slot antenna simulations performed in Part 1 was carried out using aluminum as the metal, while the routing structures was simulated in PEC. The reason for this was that some of the routing structures involving 10-12 ports would require a relatively long simulation time, a time that somewhat could be reduced by the use of PEC instead of aluminum. The antenna was simulated using aluminum due to this being one of the possible metals used for production of this type of antenna in the future.

3.2 Part 1: Gap Waveguide Automotive Radar Antenna and Transition

The method section for Part 1 includes determining appropriate goals for the performance of the single column slot antenna, and to decide which parameters that

would be appropriate to check when performing a transition tolerance analysis.

3.2.1 8-slot Single Column Antenna

There are several parameters to take into account when designing an antenna, and depending on application they all have different importance. For this work, the following goals were set:

- The aim for the side lobe level should be -20 dB, but an acceptable level is -18 dB.
- The matching of the antenna input is preffered to be -20 dB, but -18 dB is acceptable.
- The main lobe magnitude is aimed for 15 dBi.
- The 3 dB-beam width is desired to be 10° for elevation and as wide as possible for the azimuth beam width.

3.2.2 Microstrip-to-double ridge waveguide transition analysis

A layout for a microstrip-to-double ridge waveguide transtion is shown in Figure 3.1, where Figure 3.1a shows the transition with the waveguide lid and Figure 3.1b shows the microstrip patch and the substrate mushrooms.

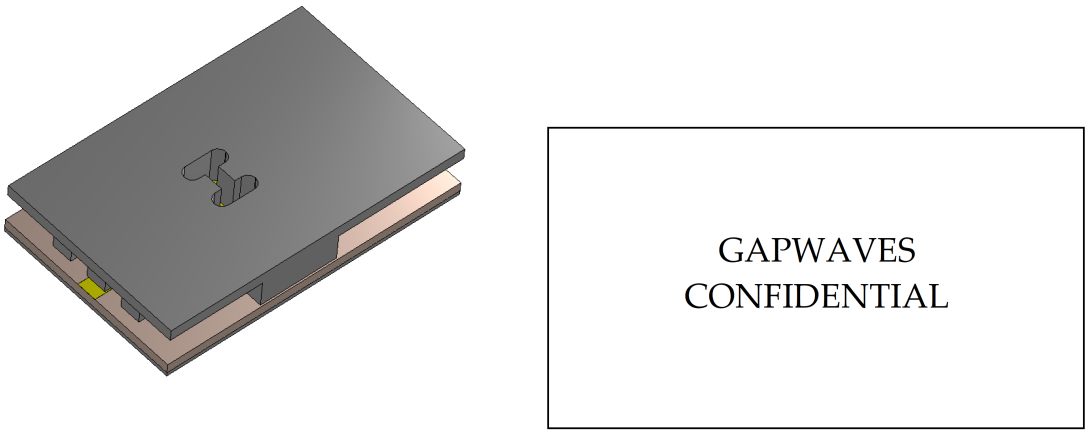

(a) With lid **(b)** Without lid

Figure 3.1: Microstrip-to-double ridge waveguide transtion. In Figure (a), the transition is shown with the waveguide lid, and in Figure (b) the patch and mushrooms can be seen.

There are several parameters that influences the performance of the transition and which could be included in a tolerance analysis. The tolerance analysis was performed by changing the value by $\pm 20\mu$m of the following parameters:

- **Pins:** The position, width and distance to the PCB (i.e. the pin height).
- **Mushrooms:** Via hole diameter, mushroom patch width, mushroom period and waveguide patch-to-mushroom separation.

- **Waveguide Lid:** Waveguide lid displacement in both x and y-direction, and the distance from the double ridge waveguide to the PCB.

The overall influence of the pins and mushrooms were also examined, as to learn why these are necessary at all for the transition performance.
It is important to state that the main aim of the tolerance analysis is not to find the best transition performance, but rather to learn which parameters affects the overall result of the transition. This will help in designing the transition best suited for a specific situation.

3.3 Part 2: Advanced Radar Solutions

There are several steps to take into consideration when examining how to route a system using gap waveguides. It was decided to start by examining hollow waveguides and how to bend such structures, and then translate this into gap waveguides.

3.3.1 Waveguide Bending compensation

Bends in the waveguide is necessary when designing large routing systems, but this bending will also degrade the system performance due to parasitic reactances introduced at such corners. It is however possible to reduce these parasitics by proper discontinuity compensation, either by smoothing the corners or by mitering the edges [7].
A figure describing the nomenclature used when examining the properties of waveguide edge mitering are shown in Figure 3.2. The waveguide width w in Figure 3.2 is one of the two fundamental waveguide widths a or b.

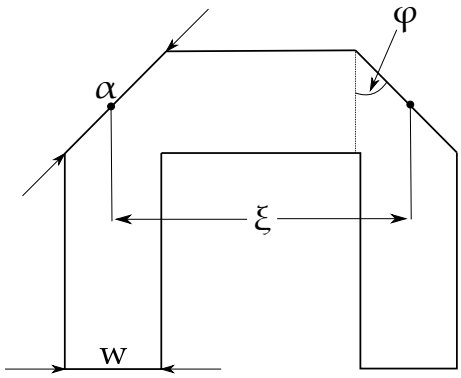

Figure 3.2: Simple figure describing the nomenclature used in examination of bends in waveguide structures. The waveguide structure is seen from above.

The bending compensation will be performed as follows: Firstly, one needs to determine which parameters α, ξ, φ, w and possibly the waveguide height h (not shown in Figure 3.2) that is appropriate in order to have low return loss and high S_{21} while using as little area as possible. This first step is performed on hollow waveguides. Secondly, what have been learned about the bending for HWGs is translated to gap waveguide structures, where parameters such as pin size and separation is determined.

3.3.2 Bending of Hollow Waveguide and Gap Waveguide

The hollow waveguide used for comparing hollow waveguide and gap waveguide bends is shown in Figure 3.3, where Figure 3.3a displays a wire frame representation of the waveguide in order to clearly see the waveguide path. The bend in Figure 3.3 is not mitered even though both mitered and not mitered corners were examined and compared for both HWG- and Gap WG-structures.

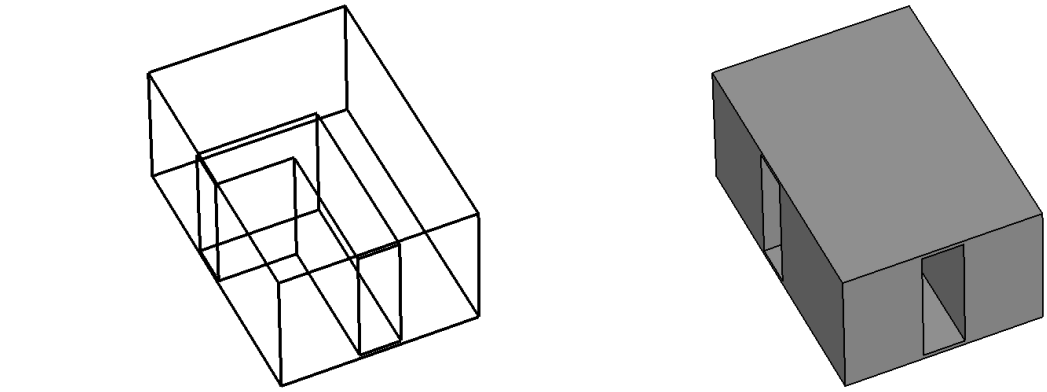

(a) Wireframe **(b)** Solid

Figure 3.3: Hollow waveguide with 90° bend. The figure is displaying a regular waveguide bend, without any mitering of the corners.

3.3.3 Space Limitation Considerations

There are several design limitations that needs to be considered when routing advanced radar systems; one of the most important ones is the limited amount of space. The radar cannot take up a large area since it needs to be implemented in already crowded locations such as the car bumper, but at the same time it can be desired to have large amount of Rx- and Tx-channels for e.g. imaging radars. It is therefore important to try to decrease the waveguide size used for routing but still having high S_{21} and low losses, and also be able to have transmission lines close to each other without high coupling.
In order to use as little space as possible, it was decided to flip the waveguide and put it with the short side b down. Even though it will increase the total height of the routing system, it allows for more transmission lines side-by-side when the routing area is small.
When decreasing the waveguide area it is necessary with a transition from standard waveguide size to the new, smaller dimensions since there may be waveguide ports connecting the radar chip with the routing layer. The transition can either be done by a step taper, which consists of one or more sections, or by using a smooth taper. The transition from standard WR12-waveguide size to the new, smaller size was first optimized for hollow waveguide and then translated to gap waveguide.

3.3.4 Pin size, separation and air gap

The pin height, width, length and spacing of the routing layer needs to be optimized both for performance and feasibility. As a rule it was said that the minimum separation between pins should be minimum 0.5 mm in order for the gap waveguide to be practical for production.

4
Results

The results are divided into two sections, corresponding to the two main parts of this thesis work; Section 4.1 is devoted to Part 1 with the design of the slot antenna and a microstrip-to-double ridge transition tolerance analysis, and Section 4.2 concerns the advanced radar solutions in terms of routing.

4.1 Part 1: Gap Waveguide Automotive Radar Antenna and Transition

In the following section, results from the single column 8-slot antenna design are presented. This section also includes reference simulations with a microstrip antenna, as well as a transition tolerance analysis.

4.1.1 Single Column Antenna Design

The single column 8-slot antenna is shown in Figures 4.1-4.4. The center-fed antenna consists of a ridge gap waveguide surrounded by pins and fed with a double-ridge waveguide input. In Figure 4.1, an exploded view of the antenna is shown with the double-ridge transition, ridge and pin layer and also the slot layer. The antenna can be considered to be similar to a resonant array, but with an open end instead of a short-circuited.

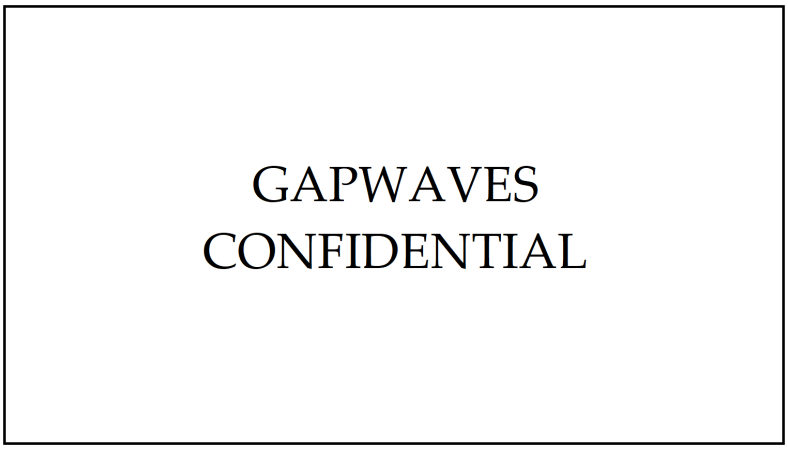

Figure 4.1: Exploded view of the single element antenna.

The pin and ridge layer is shown in Figure 4.2, where it can be seen that the ridges

are terminated with end pins of a different size compared to the pins creating the waveguide.

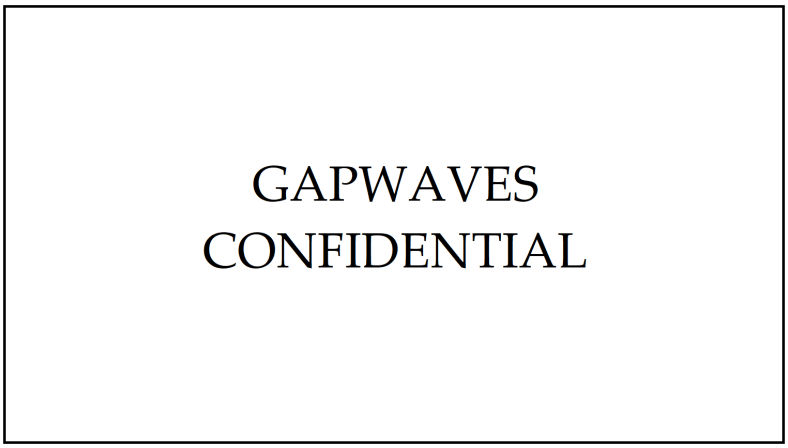

Figure 4.2: Ridge and pin-layer used in the single element antenna.

The slot layer is shown in Figure 4.3. There is a mirror symmetry to the slots from the center and out, meaning that e.g the two slots closest to the feed (Slot 1) have the same size and offset and so on. The slots are in theory separated by half a guided wavelength, but this changed slightly when allowing the optimization routine to run. The widths are equal for all slots. The total width of the whole slot layer was also adjusted as a way of increasing the beam width of the antenna.

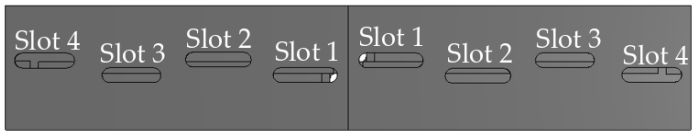

Figure 4.3: Slot-layer used in the single element antenna.

The input matching could be adjusted by finding the proper values of the height and length of the ridge step, which can be seen in Figure 4.4.

GAPWAVES
CONFIDENTIAL

Figure 4.4: Input ridge and matching for the single element antenna.

4.1.1.1 Simulation Results of Single Column Slot Antenna

The performance of the antenna described in the previous section is presented in Figures 4.5-4.8. In Figures 4.5a-4.5b, the far field elevation and azimuth patterns are shown. The main lobe gain is 14.4 dBi for both elevation and azimuth, with 3 dB beam widths of 10.2° and 106.2°. The plots show back lobes with an amplitude of 0 dBi, however these are generally not considered a problem since a real antenna would have a large ground plane which will remove these. These are thus not considered to influence the antenna performance, and instead the next highest side lobes are taken into account which results in side lobe levels of -19.2 dB.

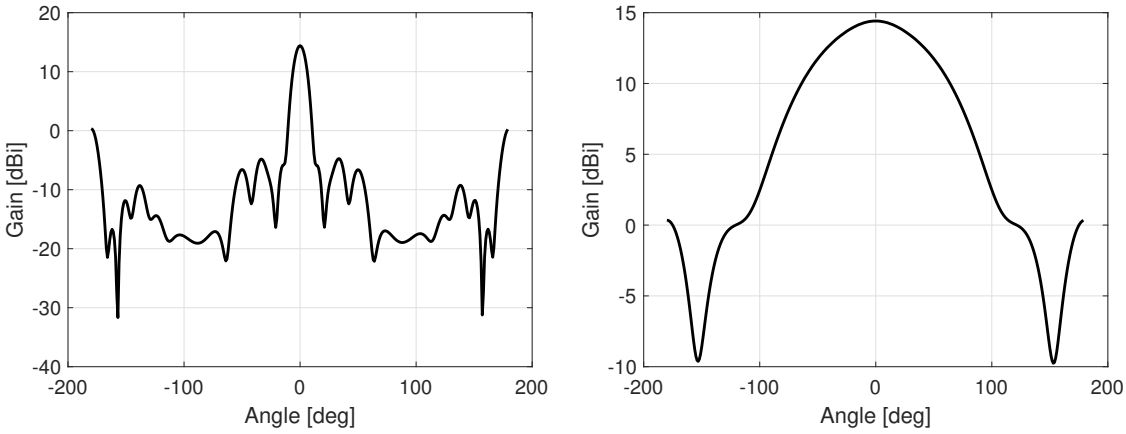

(a) Elevation. **(b)** Azimuth.

Figure 4.5: Far-field patterns for the single-column antenna at 76.5 GHz. In (a), the elevation pattern is shown, and in (b) the azimuth pattern is shown.

The input matching of the antenna is given in Figure 4.6, where it can be seen to be lower than -20 dB for the whole frequency span of 76-77 GHz.

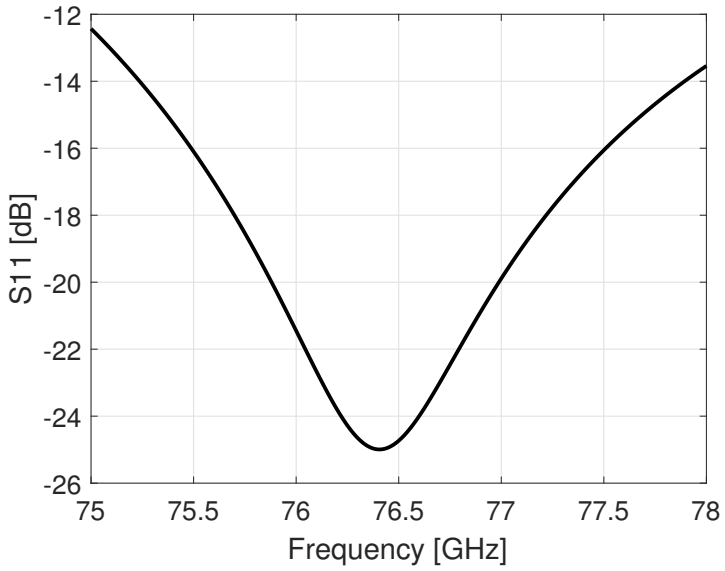

Figure 4.6: S11 for the single element antenna.

The maximum phase error of the antenna is given in Figure 4.7. It was calculated in CST by placing e-field probes on top of each slot, and then calculating the maximum phase difference between all the slots. As can be seen in the figure, the maximum phase difference in the 76-77 GHz span between all slots is 27° for 76 GHz. The phase difference can be seen as a tool for minimizing the side lobe levels of the antenna, in the sense that a lower phase difference generally means lower side lobe levels. The phase is adjusted by offsetting the antenna slots differently. Another approach in reducing side lobe levels would be to look at the e-field amplitude above all slots, since these could be optimized to be equal in order for side lobe levels to be reduced.

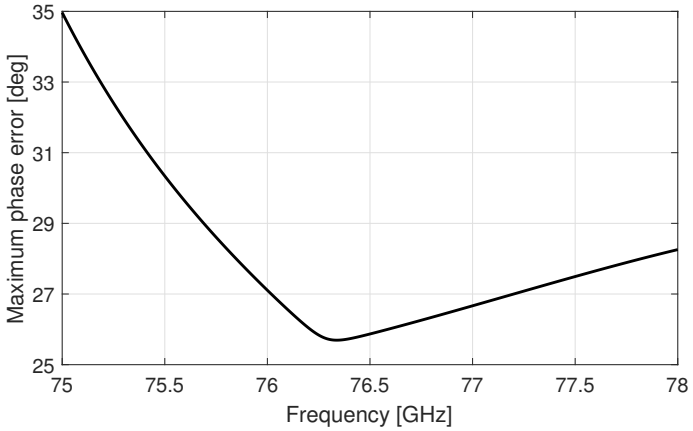

Figure 4.7: Maximum phase error for the single element antenna.

The cross polarization of the slot antenna is shown in Figure 4.8, where it can be seen to be at least 30 dB for both elevation and azimuth. It is thus regarded as a non-existing problem with unwanted polarization for this particular antenna.

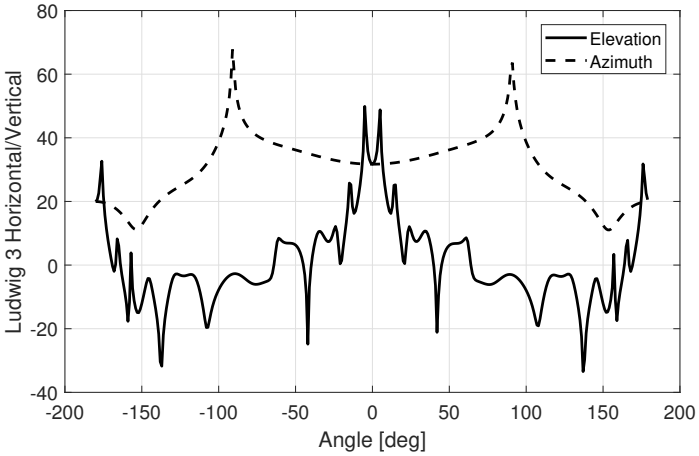

Figure 4.8: Cross polarization for the slot antenna, both in elevation and azimuth.

4.1.1.2 Microstrip Patch Reference Antenna

A microstrip patch antenna used for reference simulations is shown in Figure 4.9, and the width of each patch is given in Table 4.1. The length and width of the transmission lines connecting the patches are 1.256 mm and 0.1 mm, respectively. The substrate is RT6202, which have a relative dielectric constant of $\epsilon_r = 2.94$ [30]. The thickness of the substrate used is 0.127 mm, and the board width and length is 11.88 mm and 24 mm respectively.

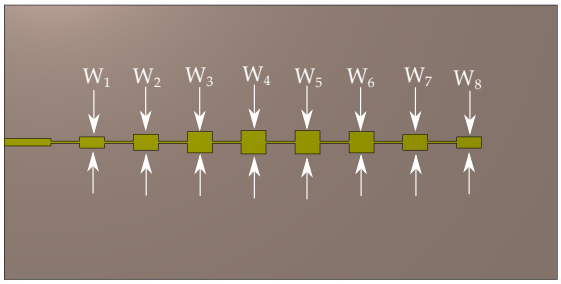

Figure 4.9: Microstrip 8-patch one column antenna used for reference.

Table 4.1: Width of each patch of the microstrip antenna.

Parameter	W_1	W_2	W_3	W_4	W_5	W_6	W_7	W_8
Length [mm]	0.485	0.7	0.933	1.01	1.01	0.93	0.67	0.485

The microstrip antenna performance is presented in Figures 4.10-4.12. Figure 4.10 shows the input matching of the antenna, which is below -7.5 dB for the span 76-77 GHz.

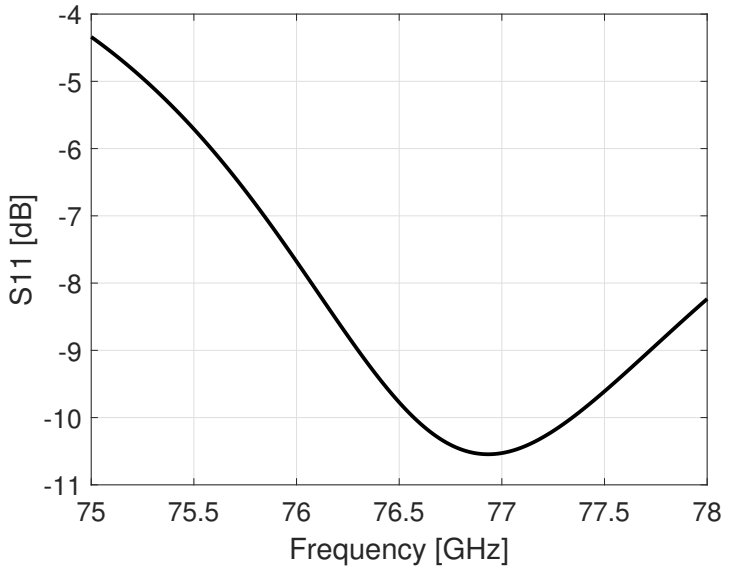

Figure 4.10: S11 of the microstrip one column antenna.

The far field pattern in elevation is shown in Figure 4.11, where it can be seen to exhibit a main lobe gain of 14.7 dBi with a side lobe level of -20.7 dB. The azimuth far field is given in Figure 4.12, which have a main lobe magnitude of 14.7 dBi as well but with a side lobe level of -31 dB. The 3 dB beam width of the elevation and azimuth beams are 11° and 80°, respectively.

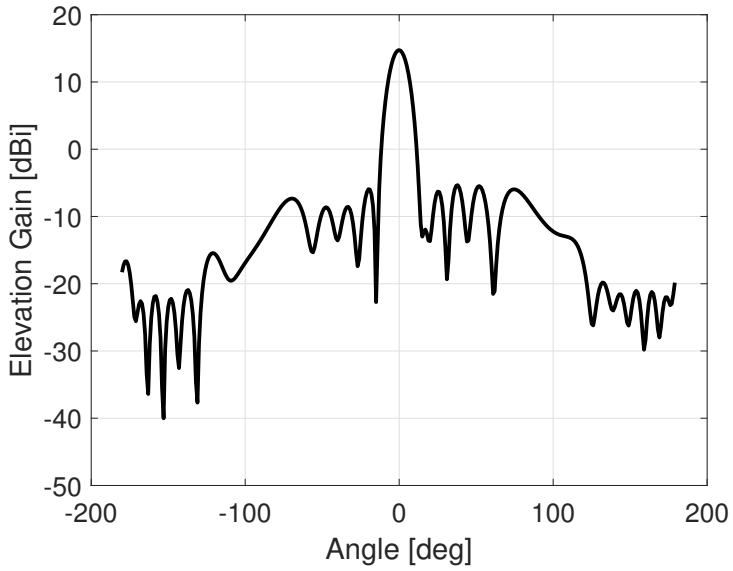

Figure 4.11: Elevation far field of the microstrip one column antenna.

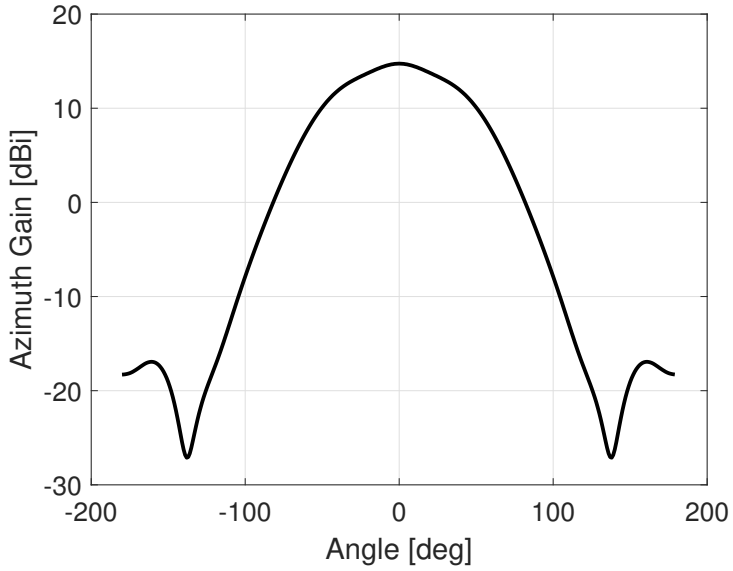

Figure 4.12: Azimuth far field of the microstrip one column antenna.

4.1.1.3 Single Column Antenna for Manufacturing and Measurements

In order for measurements to be possible, the antenna needs to be put into a frame with an adapter to a standard WR12 waveguide. This frame is shown in Figure 4.13. The antenna was not further optimized for this setup, but only placed into the frame as to see how this effected its performance.

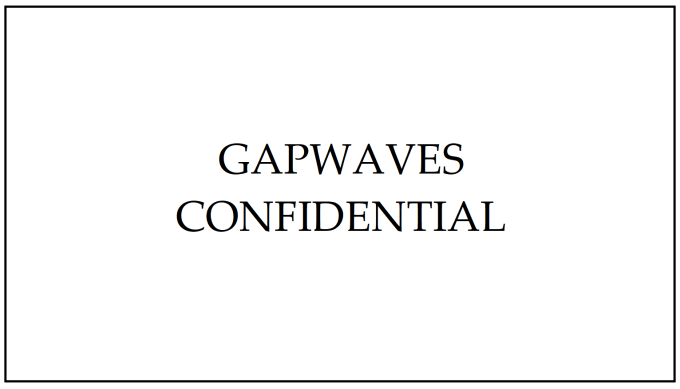

Figure 4.13: Exploded view of the single column antenna with frame.

The performance of the antenna with frame is shown in Figures 4.14-4.15 where the input matching is shown in Figure 4.14, the elevation far field in Figure 4.15a and the azimuth far field in Figure 4.15b.

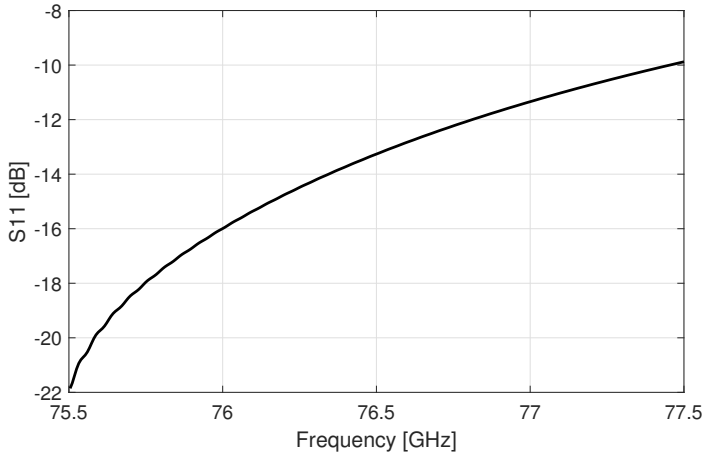

Figure 4.14: S11 for the single column antenna with frame.

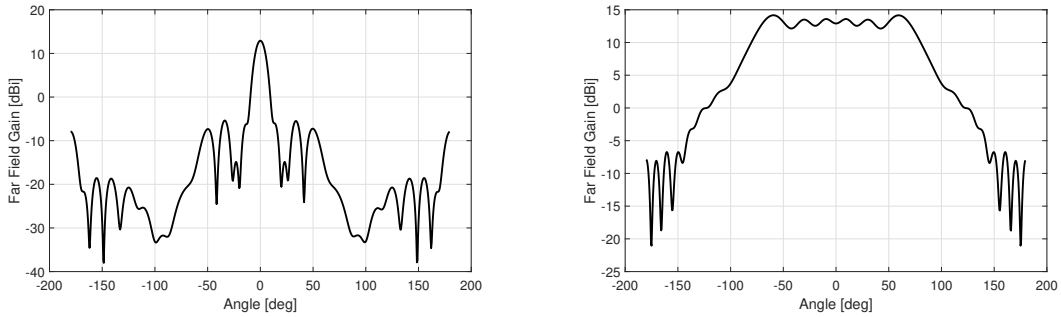

(a) Elevation **(b)** Azimuth

Figure 4.15: Far Field simulations showing the (a) Elevation and (b) Azimuth pattern.

4.1.2 Antenna Array using the 8-slot Antenna Column

There are several ways of positioning the individual antenna columns to create an array. It was decided to use 3 Tx and 3 Rx-channels, configured as shown in Figures 4.16-4.17. The columns were directly duplicated from the designed single element antenna and the size of the array is 35.3 mm x 25.3 mm.

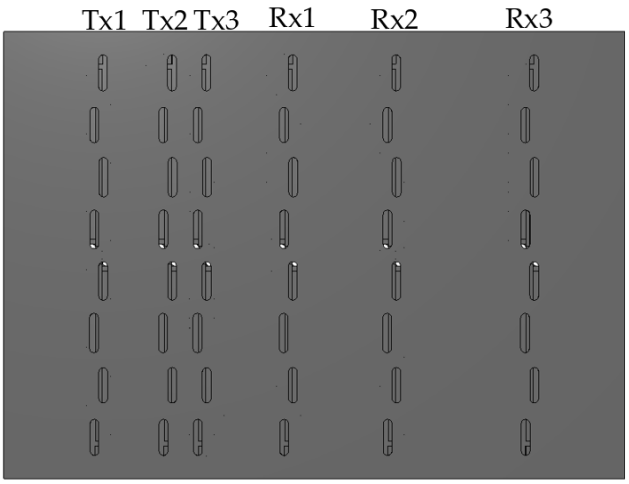

Figure 4.16: Slot array configuration.

As can be seen in Figure 4.17, since the column was duplicated but with the different separation distances between columns it meant that for Tx 2 and Tx 3 the pins were overlapping resulting in slightly larger pins between these two columns. It was decided to keep these larger pins, in order for the waveguide to maintain its original size for these two channels. The larger pins have a width of 0.59 mm and comparing this with the original pin sizes of 0.55 mm it will most likely not result in a huge difference in terms of antenna performance or manufacturing difficulty.

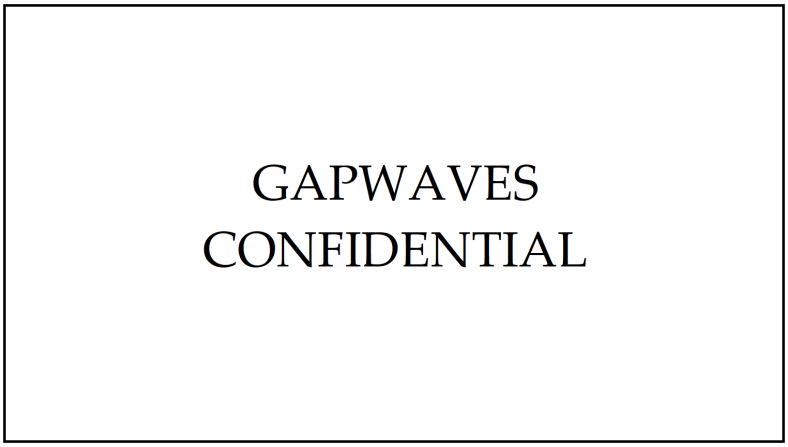

Figure 4.17: Slot array configuration, without the slot layer.

4.1.2.1 Microstrip Patch Reference Antenna Array

The microstrip reference antenna array is shown in Figure 4.18, where the columns have the same separation as for the slot antenna array. The substrate type and thickness is the same as for the single column microstrip patch antenna, i.e. susbtrate RT6202 with a 0.127 mm thickness. The total size of the whole antenna array amounted to 37.1 mm x 24.0 mm.

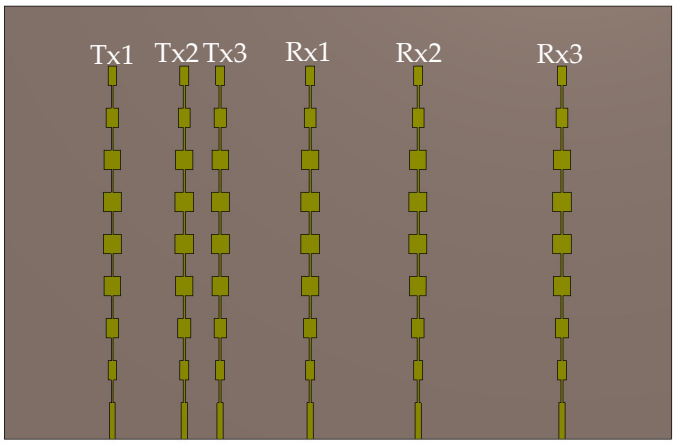

Figure 4.18: Antenna array with microstrip columns.

Simulation results for both the slot array and the microstrip array is presented in Appendix A, and a comparison of their performance is performed in Chapter 5: Discussion.

4.1.3 Transition Tolerance Analysis

The transition tolerance analysis yielded a large number of results, which is why it was decided to place them in an appendix. The results can be seen in several figures in Appendix B. It was firstly necessary to see why the pins and mushrooms were needed at all, and this is shown in Figures 4.19a-4.20 where the S-parameter performance is presented.

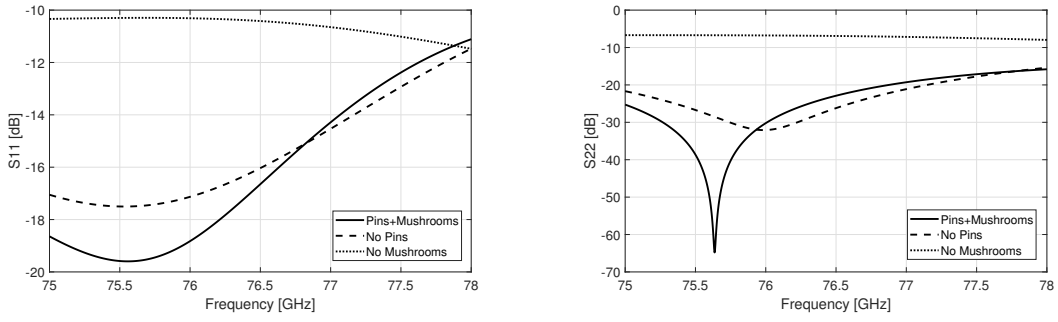

(a) S11 **(b)** S22

Figure 4.19: Pin and mushroom-influence on the port matching.

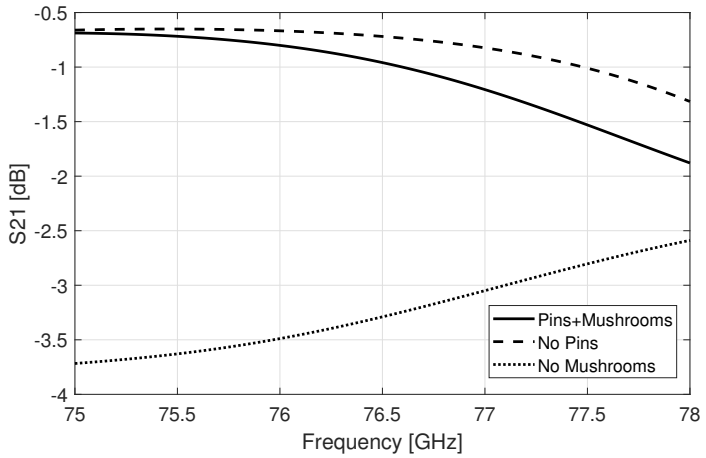

Figure 4.20: Pin and mushroom-influence on the S21-performance.

A full discussion of the transition tolerance analysis is presented in Chapter 5.

4.2 Part 2: Advanced Radar Solutions

This section presents the examination of gap waveguide structures for routing complex systems. Three different types of gap waveguides are presented, with their respective test structure simulation results.

4.2.1 Reducing the Gap Waveguide Size

The results from reducing the gap waveguide compared to a WR12-sized wavegude is presented below.

4.2.1.1 Comparison with a Microstrip Transmission Line

The starting point for the gap waveguide size was set to a = 2.8 mm and b = 0.9 mm. This smaller size compared to the standard WR12-size was chosen since it would allow for easier routing without compromizing the waveguide performance to a large extent, and was used for determining the governing laws of bending and routing with gap waveguides. A comparison of the smaller gap waveguide and a microstrip transmission line is given in Figures 4.21a - 4.21b. The substrate used for the microstrip line was RT6202 (same as for the microstrip reference antenna), where the substrate thickness was set to 0.127 mm and the microstrip width was 0.5 mm. The total length of both the Gap Waveguide and the microstrip was 16.8 mm. The design parameters used for the structure is given in table

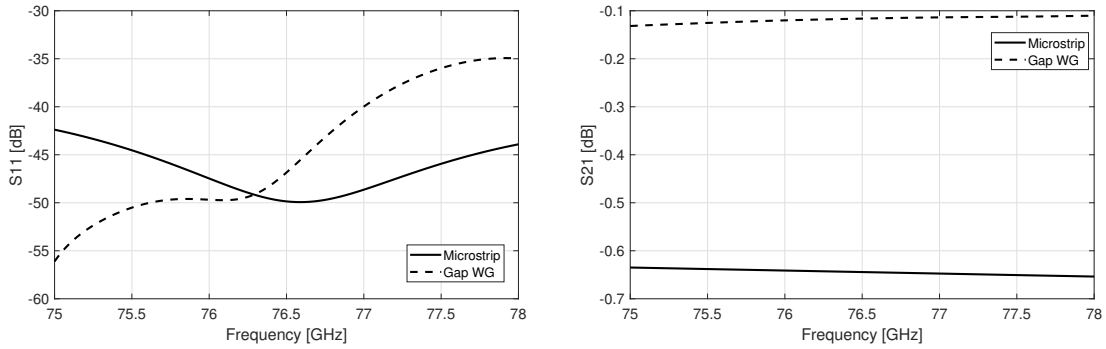

(a) S11 **(b)** S21

Figure 4.21: S-parameter performance for microstrip and gap waveguide transmission lines.

Parameter Name	Value [mm]
a	2.8
b	0.9
Pin Height	0.95
Pin Width	0.87
Pin Length	0.87
Pin Separation	0.9
Air gap	0.05

Table 4.2: Caption

4.2.1.2 Gap waveguide bending optimization

The gap waveguide structure is shown in Figure 4.22, where Figure 4.22a shows the waveguide from above and Figure 4.22b highlights the waveguide and the mitered corner. The total waveguide physical length is approximately 13.2 mm from port to port, and the mitered corner parameter α is equal to 1.06 mm.

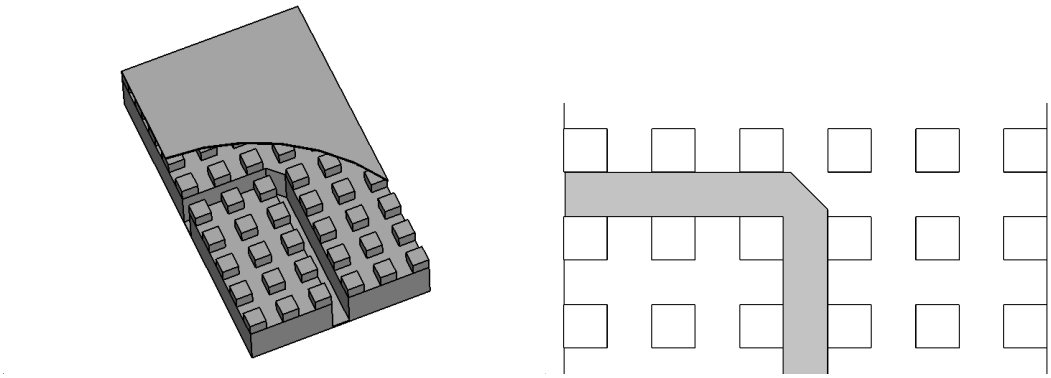

(a) Top view **(b)** Up close

Figure 4.22: Gap waveguide with 90° mitered corner. Figure (a) depicts the wavegude from the top, and Figure (b) shows the bending and mitered corner from above with the waveguide marked in grey.

Figures 4.23-4.24 shows the performance of the mitered waveguide in terms of S11 and S21. It can be seen from these figures that the mitered corner holds a significantly better performance compared to a non-mitered corner using this gap waveguide structure.

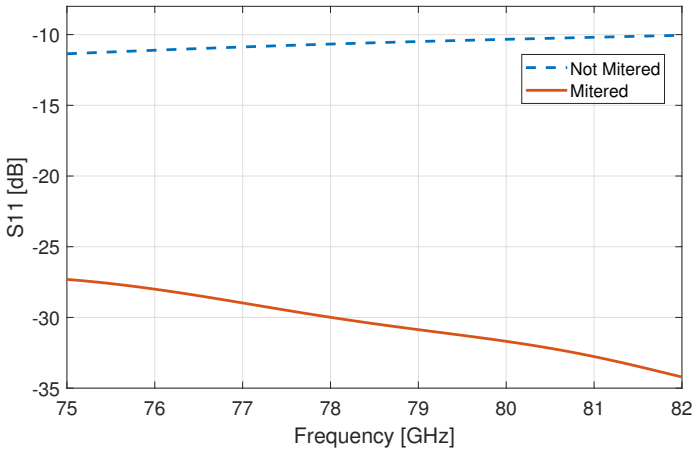

Figure 4.23: S11 of mitered gap waveguide compared with a non-mitered structure.

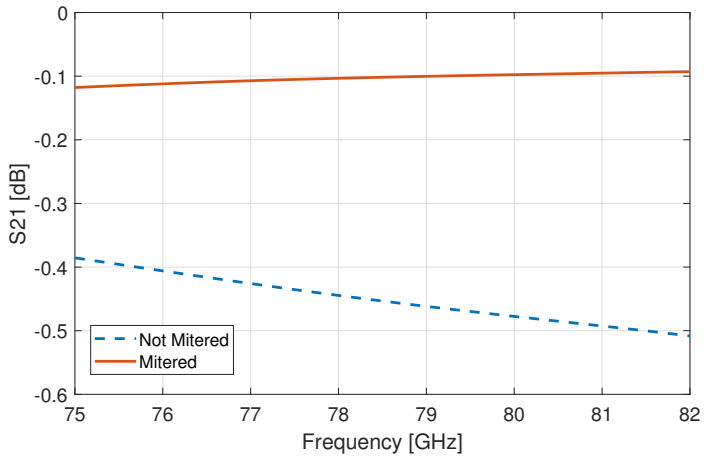

Figure 4.24: S21 of mitered gap waveguide compared with a non-mitered structure.

The E-field inside the bended waveguide is shown in Figure 4.25, where it can be seen that the field follows the bend as desired.

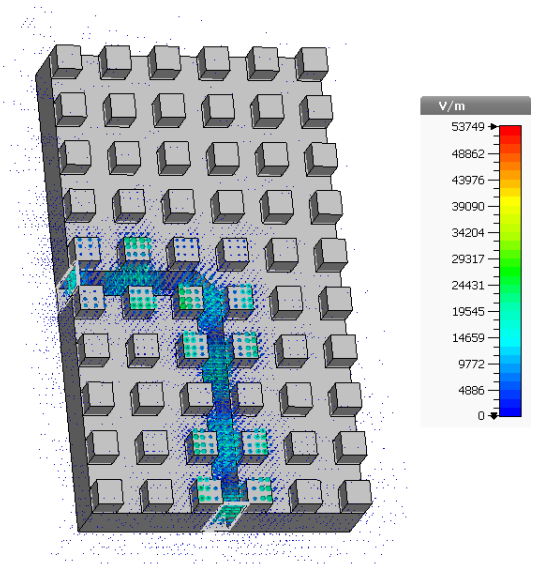

Figure 4.25: E-field of the gap waveguide bend.

4.2.1.3 Coupling between adjacent gap waveguide transmission lines

For complex routing systems, it is necessary to be able to have transmission lines close together while maintaining a low coupling. A simple model with two straight transmission lines were created, using the same design parameters as previously. This structure is shown in Figure 4.26, where the four ports are indicated.

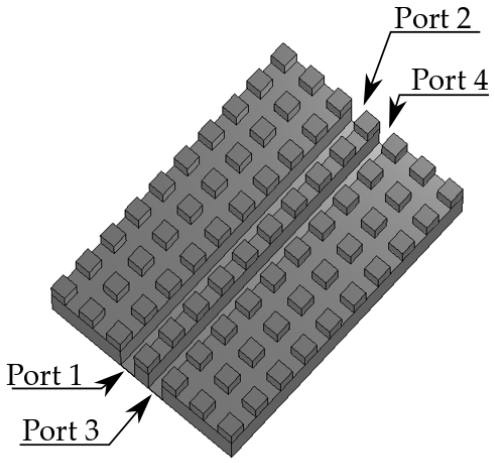

Figure 4.26: Two gap waveguides in close proximity, with the respective ports indicated.

The number of pin rows will influence the coupling between transmission lines, since more pin rows means the field will be cancelled outside the waveguide to a greater extent. The simulations were performed with a pin-to-lid air gap of 50 μm. The S-parameter performance of a two transmission line structure with either one or two rows of pins are shown in Figure 4.27. From the simulation results it can be seen that using two rows of pins will increase the performance of the system for all S-parameters, since it means a lowering of reflections (S11), better transmission coefficient (S21), lower adjacent port coupling (S31) and lower coupling between transverse ports (S41).

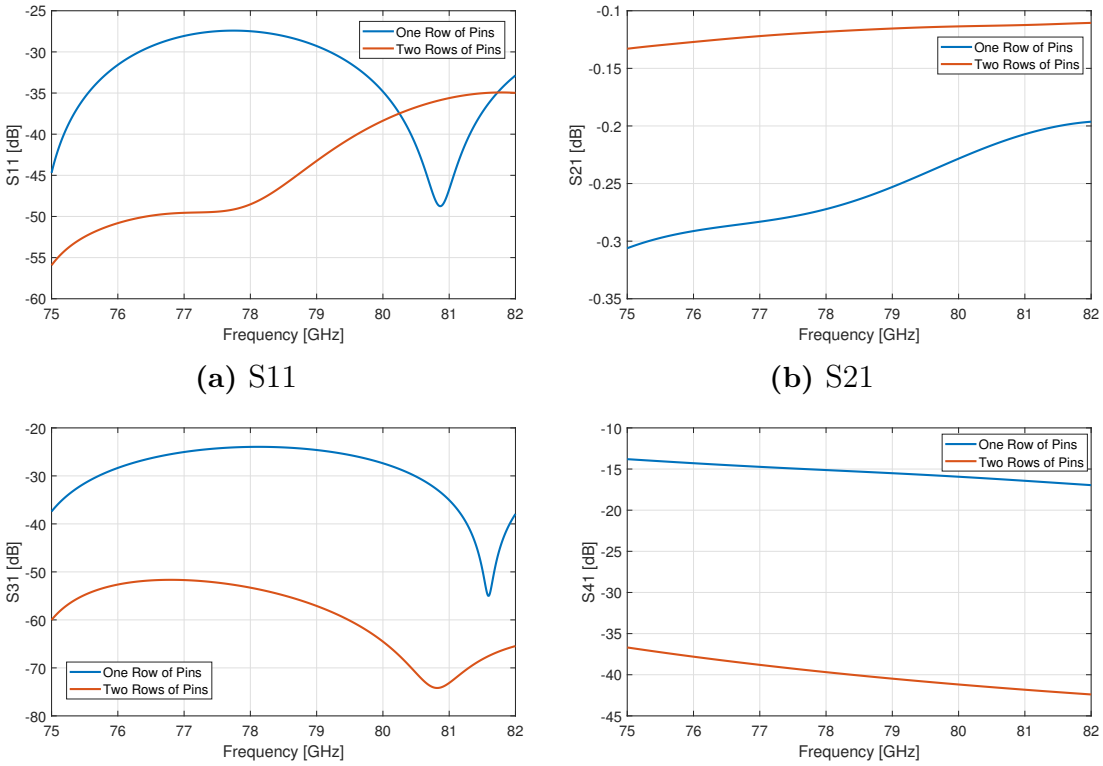

(a) S11 **(b)** S21

(c) S31 **(d)** S41

Figure 4.27: S-parameter performance of two gap waveguides separated by either one or two pin rows.

There may be routing systems where the space is very limited, and it would be desired to use only one row of pins in between transmission lines. From Figure 4.27d it is seen that waveguides separated by only one row of pins will have a couping of -15 dB for an air gap of 50 μm, which may be considered high. In order for lower coupling to occur and overall better system performance, a lower gap between the pins and lid can be used. These simulation results are shown in Figure 4.28, where it can be seen that a smaller air gap gives better results. The drawback is that the structure will be sensitive to manufacturing errors, since an increase in air gap from 10 μm to 25 μm means increasing S11, S31 and S41 by tens of dB. An increase from 25 μm to 50 μm will not have that same drastic effect on the system, and is thus less sensitive to production and assembly errors.

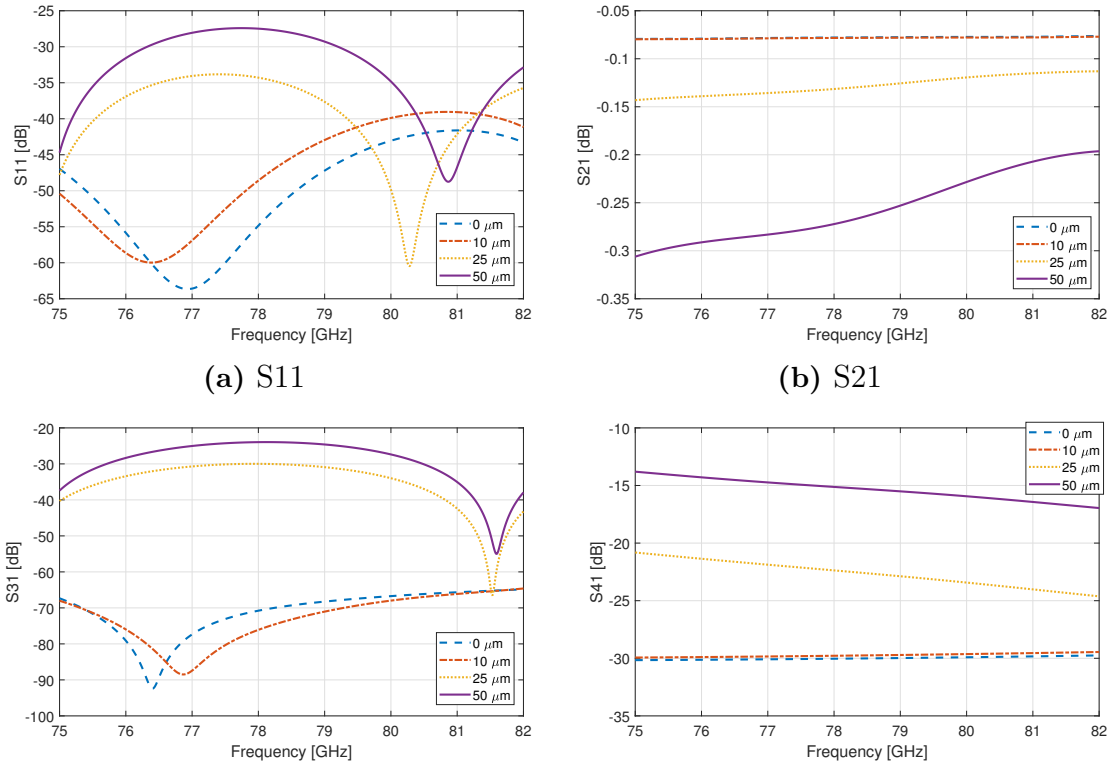

(a) S11 **(b)** S21

(c) S31 **(d)** S41

Figure 4.28: S-parameter performance of a two-line gap waveguide separated by one row of pins.

4.2.2 Routing Type I: Smaller Gap Waveguide Cut from Bed of Pins

A transition from standard WR12 to the new smaller waveguide size was developed and is shown in Figure 4.29 as a part of a back-to-back gap waveguide. The transition was decided to be a two-step transition to get a better performance. The waveguide and pin sizes were optimized in combination with several other parameters in order to improve the performance, which gave a waveguide size of a = 2.91 mm and b = 1.07 mm. First the bed of pins were constructed, and then the waveguide was simply cut from the structure resulting in pins with a smaller width of 0.51 mm closest to the waveguide.

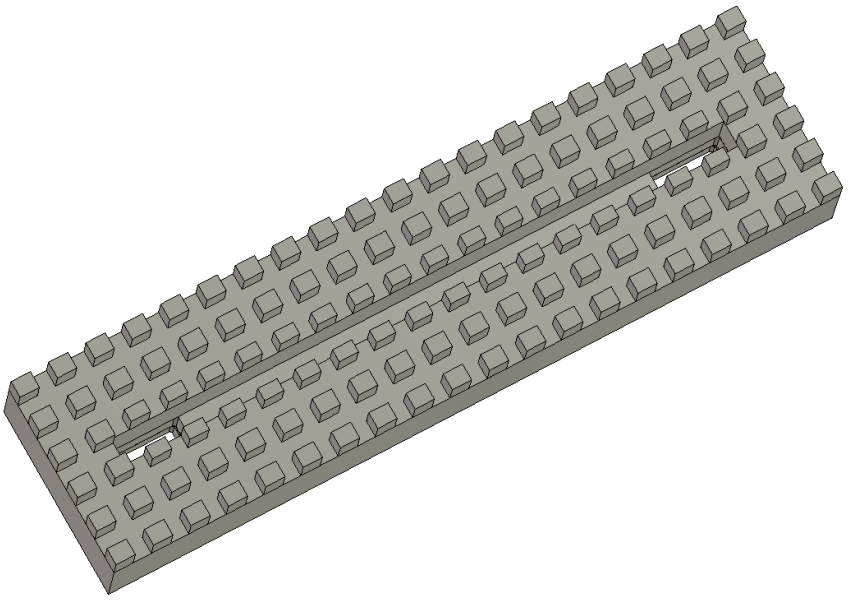

Figure 4.29: Tapered transition to smaller waveguide as seen from above.

A wireframe view of the transition is shown in Figure 4.30.

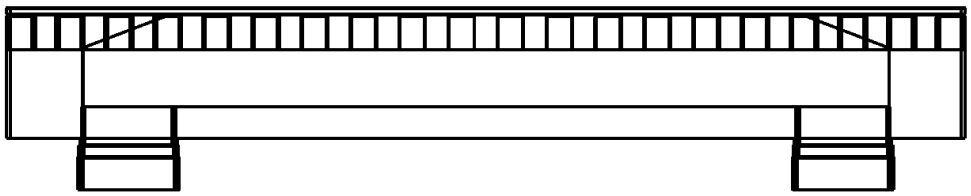

Figure 4.30: Wire frame view of B2B-waveguide including taper from WR12 to new, smaller size.

Different parts of the transition is shown in Figure 4.31, where in Figures 4.31b and 4.31d the design parameters are highlighted. A wedge was used above the ports in order to give a better matching, where the width of the wedge was equal to the waveguide size b and the height of the wedge was set equal to the pin height.

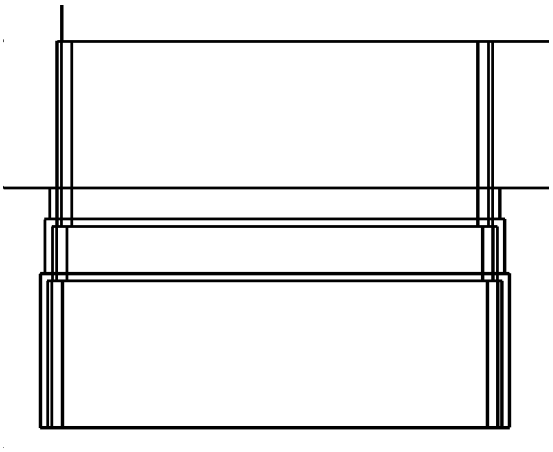

(a) Taper close-up (side view)

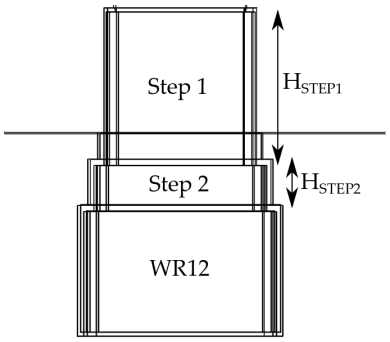

(b) Taper close-up (front view)

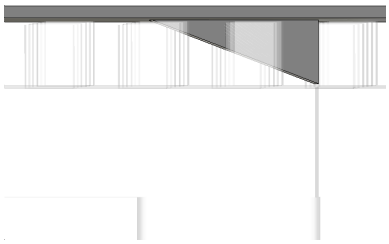

(c) Lid Wedge

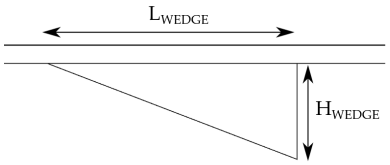

(d) Lid Wedge (Side View)

Figure 4.31: Selected parts of the transition: Figure (a) shows the taper from the side, (b) is a front view of the taper with height variables indicated and (c) is a display of the matching wedge used. Figure (d) shows the parameters of the wedge, where the width w_{WEDGE} is not displayed.

The design parameter values used in simulations are given in Table 4.3.

Table 4.3: Parameter values used for simulations.

Parameter name	**Value [mm]**
b	1.07
a	2.91
H_{STEP1}	1.26
H_{STEP2}	0.371
H_{WR12}	1
H_{WEDGE}	1.05
L_{WEDGE}	2.74
W_{WEDGE}	b
Pin Height	1.05
Pin Width	0.67
Pin Length	0.80
Pin Separation	0.75

4.2.2.1 Tapering and Matching Lid Wedge

The performance with tapering and wedge in three different combinations are given in Figure 4.32. A significant lowering of S11 was obtained by introducing a wedge in the lid above the waveguide port. The use of tapering will also give a higher performance compared to a non-tapered structure. It is therefore suggested that both wedge and two-step taper should be used in a routing system where transition from WR12 to smaller waveguide sizes are needed.

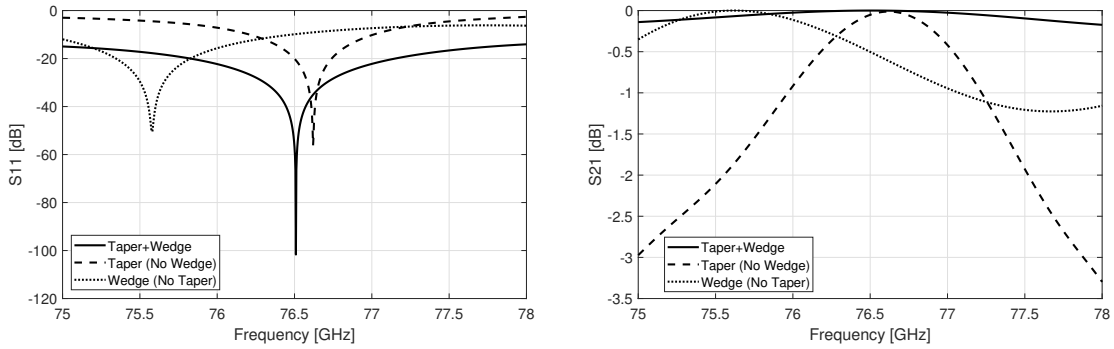

(a) S11 **(b)** S21

Figure 4.32: S-parameter performance of a B2B-gap waveguide with tapered transition from WR12 and matching lid wedge. The performance is compared to the cases if no taper or matching lid is used.

4.2.2.2 Type I Test structure

A test structure was designed with the transition, matching wedge and smaller waveguide and this is shown in Figure 4.33. This was constructed in order to determine how the waveguide separation impacted on the results and how ports aligned at 45° would perform. As previously, the wave guide itself was cut from a bed of pins and the pins may thus not be symmetric around the waveguide itself. It was also decided to examine both 10 and 50 μm air gap between the pins and the lid in order to see how the coupling would change with an air gap change.

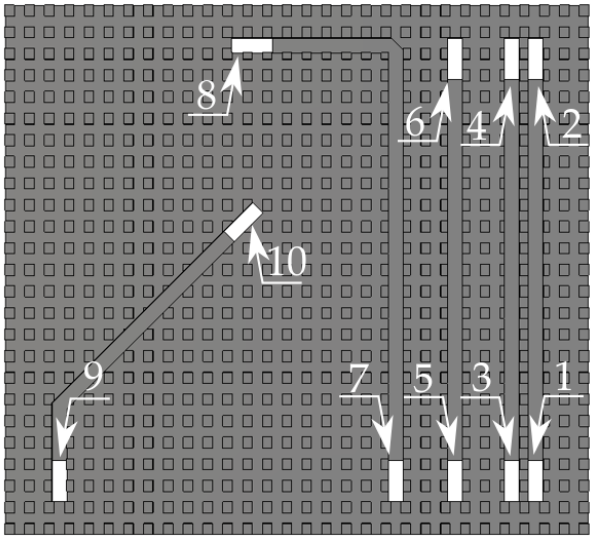

Figure 4.33: Test structure designed for the non-symmetric smaller waveguide.

The performance of the test structure is shown in Figures 4.34-4.37. In Figure 4.34, the coupling between adjacent ports i.e. neighbouring ports are shown for transmission lines separated by approximately 1 or 2 rows of pins, using 10 or 50 μm of air gap between the pins and the lid. The results show that for a smaller air gap, the coupling will be lower. A larger distance between the neighbouring ports will also result in lower coupling regardless of air gap.

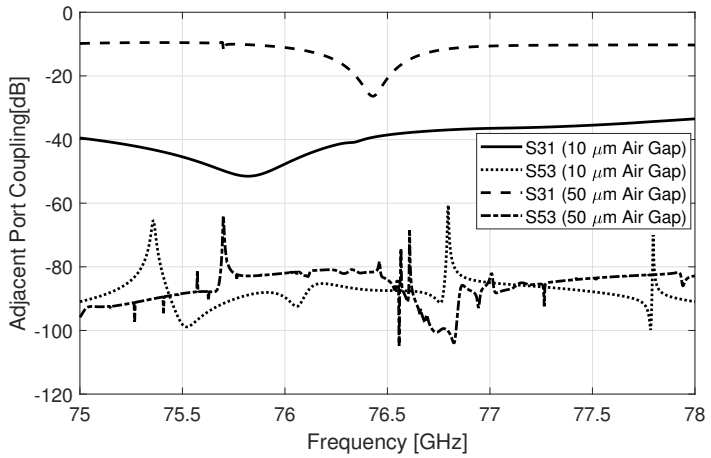

Figure 4.34: Adjacent Port Coupling for ports 3-1 and 5-3.

The opposite port coupling is shown in Figure 4.35, for ports 4-1 and 6-3. This examines the unwanted coupling between transmission lines, and is generally below -40 dB when the air gap is 10 μm. The coupling between transmission lines separated by approximately one row of pins will be higher than -20 dB for a larger air gap.

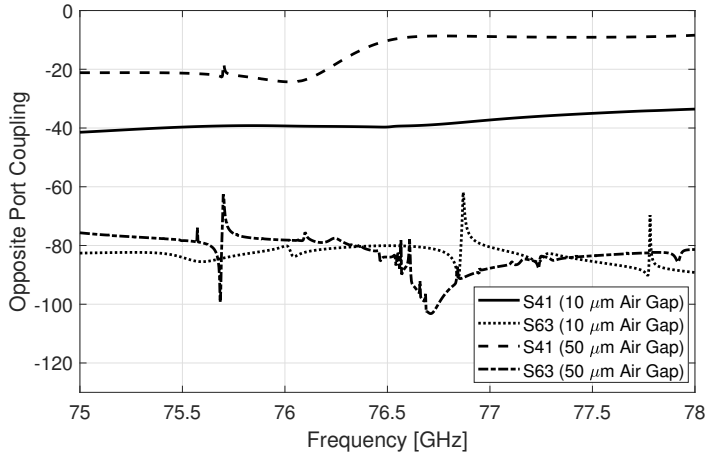

Figure 4.35: Opposite Port Coupling for ports 4-1 and 6-3.

The input matching of ports 1 and 10 are shown in Figure 4.36 for both air gaps. It is clear from the results that the input matching is worsened by tilting the port 45°, since it is -15 dB for 76 GHz where the vertical port have a matching below -20 dB for the whole span.

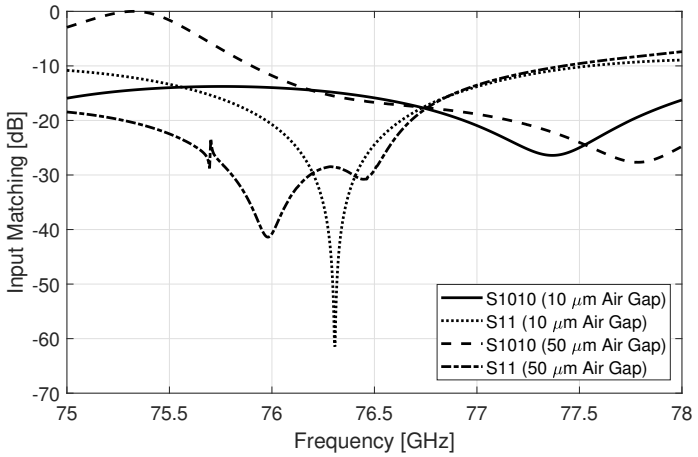

Figure 4.36: Input matching for ports 10 (aligned 45°) and 1.

The transmission coefficient is shown in Figure 4.37 for a straight line (ports 5-6), 90° bend (ports 7-8) and 45° bend. As previously, the performance is affected negatively by an increase in the air gap. It is also seen that for the 45°-port, the losses are a bit larger for the center frequency but 0.2 dB or lower for the whole span. The 45°-port transmission line is however more sensitive to an air gap change compared to the other transmission lines, since there is a large dip in througput for the 50 μm-scenario.

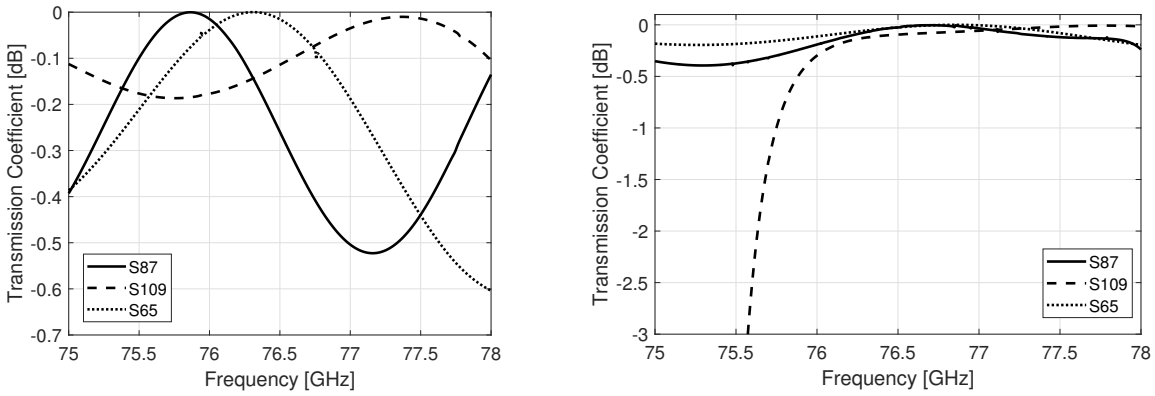

(a) 10 μm **(b)** 50 μm

Figure 4.37: Transmission Coefficient for transmission lines with ports 5-6, 7-8 and 9-10. In (a), the air gap between pins and lid is 10 μm and in (b) the air gap is 50 μm.

4.2.3 Routing Type II: Smaller Gap Waveguide with Pins aligned to Waveguide Edges

Positioning the pins at the edges of the waveguide results in equally sized pins for the whole structure, but it might be more difficult to produce especially when wishing to bend the waveguide. A B2B-structure like this is shown in Figure 4.38, which also have a two-step transition to WR12 and a mathcing wedge in the lid (not displayed).

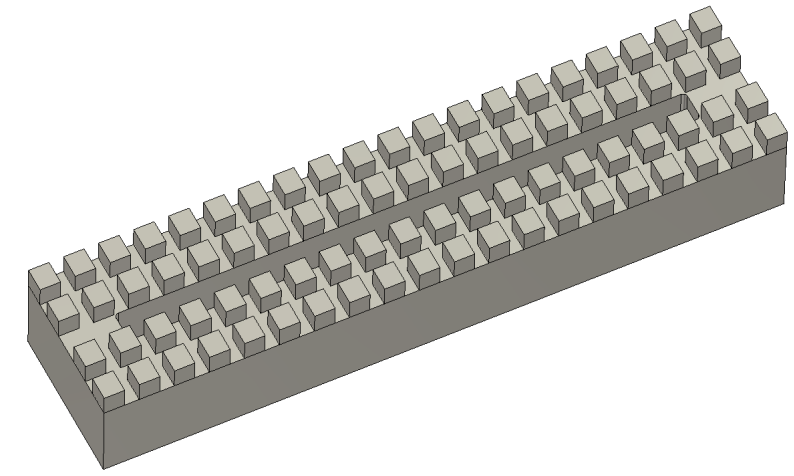

Figure 4.38: Waveguide with transition from WR12 to smaller waveguide size, where the pins are located exactly at the waveguide edge.

The parameters used for this transition is given in Table 4.4.

Table 4.4: Parameter values for the transition with pins at the waveguide edges.

Parameter Name	Value [mm]
a	2.88
b	1.1
H_{STEP1}	1.66
H_{STEP2}	1.21
H_{WR12}	1
H_{WEDGE}	Pin Height
L_{WEDGE}	3.7
W_{WEDGE}	b
Pin Height	0.802
Pin Width	0.844
Pin Length	0.719
Pin Separation	0.510

The performance of this transition is shown in Figures 4.39a-4.39b, using an air gap of 10 μm between pins and lid. The input matching is below -13 dB for 76-77 GHz, and is quite narrowband which would indicate the need for further tapering.

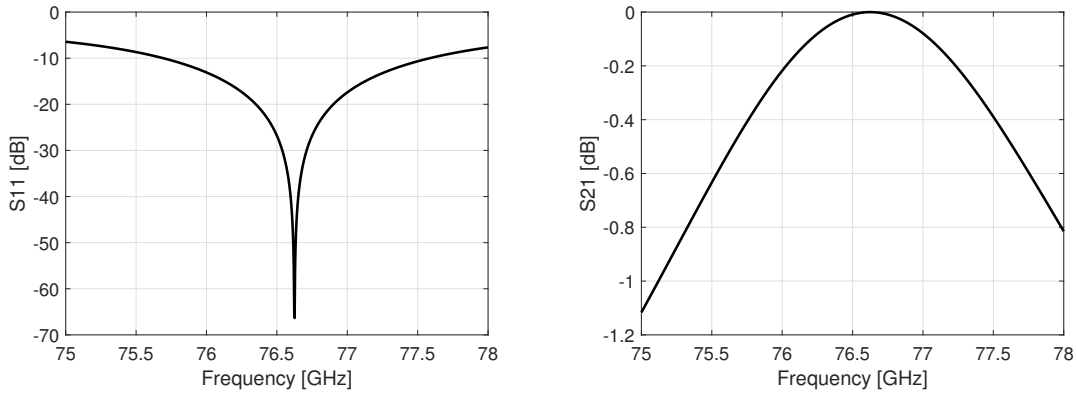

(a) S11 **(b)** S21

Figure 4.39: S-parameter performance of the taper B2B-structure with pins positioned at the edges of the waveguide.

4.2.3.1 Type II Test Structure

A test structure designed for Type II routing is shown in Figure 4.40. The test structure was only simulated for an air gap between pins and lid of 10 μm, since there is a clear idea of how the air gap affects the coupling from previous simulation results.

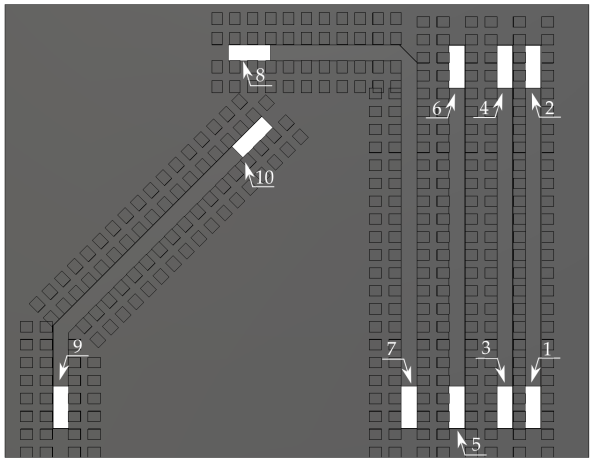

Figure 4.40: Test Structure for Type II routing structure.

The simulation results are shown in Figures 4.41-4.42. In Figure 4.41a the port return loss is shown for ports 1 and 10, and in Figure 4.41b the transmission coefficient is displayed for lines 5-6, 7-8 and 9-10. The return loss is quite high, above -10 dB for both ports displayed, and the transmission coefficient is below -1 dB for almost all frequencies and lines. This shows that there may be large losses in the system.

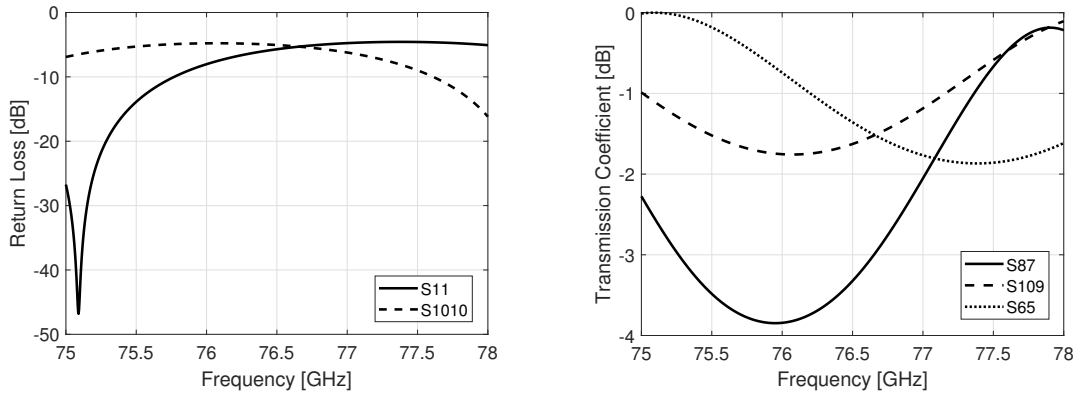

(a) Return Loss **(b)** Throughput

Figure 4.41: Return loss (a) and Transmission Coefficient (b) of the Type II test structure.

In Figure 4.42a, the coupling between neighbouring ports are given and can be seen to be lower when two rows of pins are used to separate the transmission lines. The opposite port coupling is shown in Figure 4.42b and as for the adjacent port coupling it is significantly lower when using two rows of pins between lines.

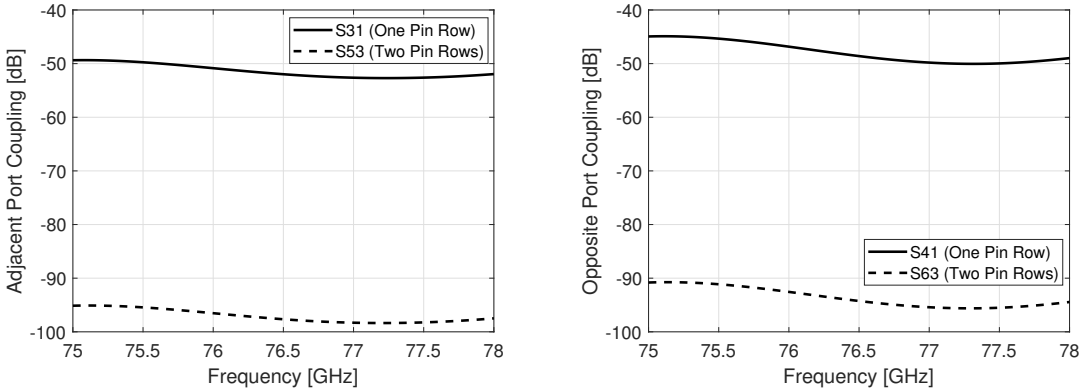

(a) Adjacent **(b)** Opposite

Figure 4.42: Coupling of the Type II test structure: (a) shows the adjacent port coupling, and (b) shows the opposite port coupling.

4.2.4 Routing Type III: WR12-Gap Waveguide with Pins aligned to Waveguide Edges

Another routing approach would be to use the regular WR12 waveguide size, which would remove any need of tapering. This would however result in a larger waveguide, which can be a problem for complex routing systems with a need for many transmission lines. The back-to-back waveguide is shown in Figure 4.43, which also includes a matching wedge in the lid (not displayed). This routing will also differ from the previous setup in that it is symmetric, i.e. the pins are placed at the waveguide edges and are thus all the same size. There is also end pins positioned at the short edges, and these are currently the same size as the other pins.

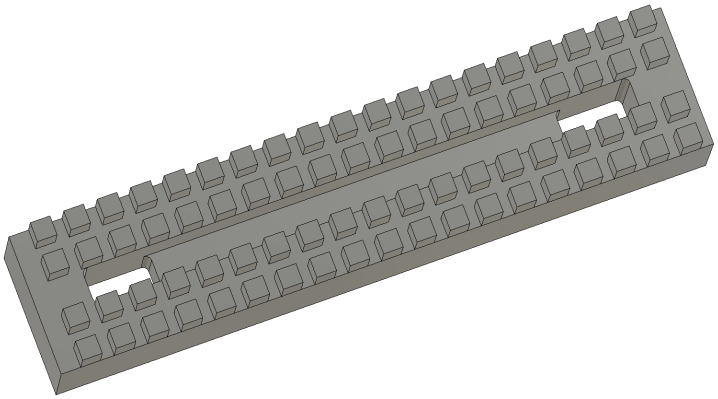

Figure 4.43: Waveguide structure with standard WR12-waveguide size.

The parameters and their specific values used in the WR12-routing is given in Table 4.5.

Table 4.5: Parameter values for the WR12-routing.

Parameter Name	Value [mm]
a	3.0988
b	1.5494
H_{WEDGE}	Pin Height
L_{WEDGE}	2.66
W_{WEDGE}	b
Pin Height	1.29
Pin Width	0.841
Pin Length	0.860
Pin Separation	0.605

The performance of the waveguide in terms of S11 and S21 is shown in Figures 4.44a-4.44b. The simulation results are for air gaps 0, 10 and 50 μm between pins and lid. The structure shows an S11 of below -17 dB for the whole frequency span of 76-77 GHz, but some resonances occur at 77.5 GHz when using an air gap of 50 μm.

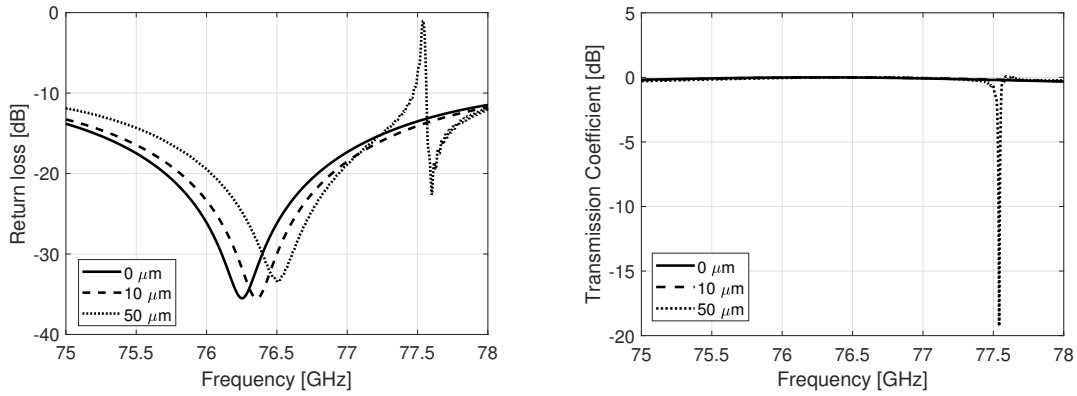

(a) S11 **(b)** S21

Figure 4.44: Simulated performance of the WR12-routing B2B-structure.

4.2.4.1 Type III Test Structure

A test structure for the WR12-sized gap waveguide was constructed and is shown in Figure 4.46. It consisted of 6 transmission lines with one or two rows of pins, where the pins were aligned with the waveguide edges. As previously, matching wedges attached to the lid were used but these are not displayed in Figure 4.46. Transmission lines 1-2, 3-4 and 5-6 were used to see the effect of coupling between transmisson lines separated by either one or two pin rows. Transmission line 7-8 was designed to see how a 90° mitered bend would behave, and transmission lines 9-10 and 11-12 were used to examine the behaviour of 45°-ports for different positions of the pins. The air gap between pins and lid were 10 μm.

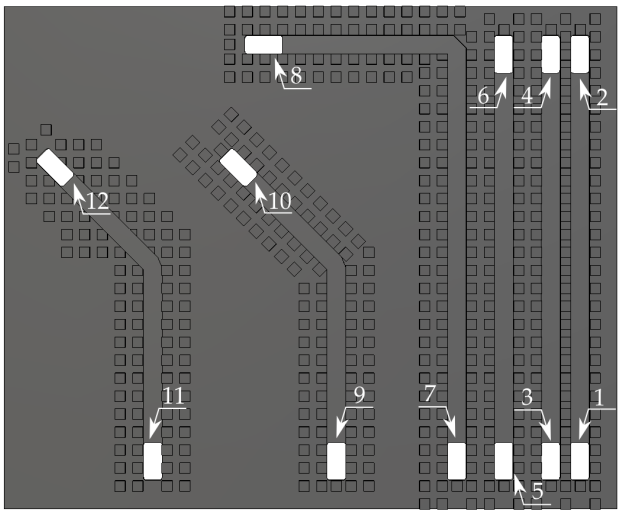

Figure 4.45: Test Structure for WR12-sized Gap Waveguide routing.

The main results from the test structure is given in Figures 4.46a-4.46c.

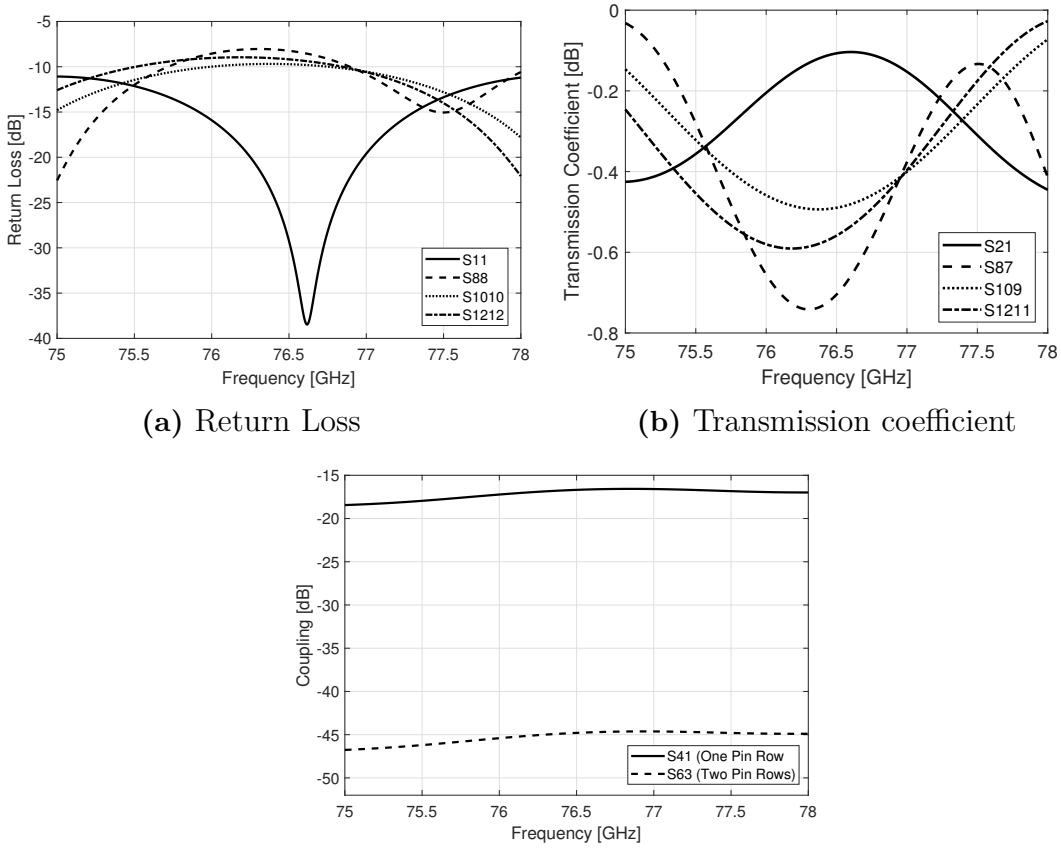

(a) Return Loss

(b) Transmission coefficient

(c) Coupling

Figure 4.46: Return Loss, Transmission coefficient and Coupling of the WR12-test structure.

Figure 4.46a shows the port return loss for ports 1, 8, 10 and 12. This is to examine how the 90°- and 45°-bending affects the return loss of the ports. The transmission coefficient in Figure 4.46b is for line 1-2 and the three lines with bends. The coupling is examined for lines 1-2 to 3-4 and 3-4 to 5-6, i.e. straight lines separated by one or two rows of pins.

4.2.5 Matching Wedge Tolerance Analysis

In order to determine which effects any assembly errors might have on the performance due to the position of the wedge, a short tolerance analysis was performed in xy-direction. The direction of the x- and y-displacement is shown in Figure 4.47.

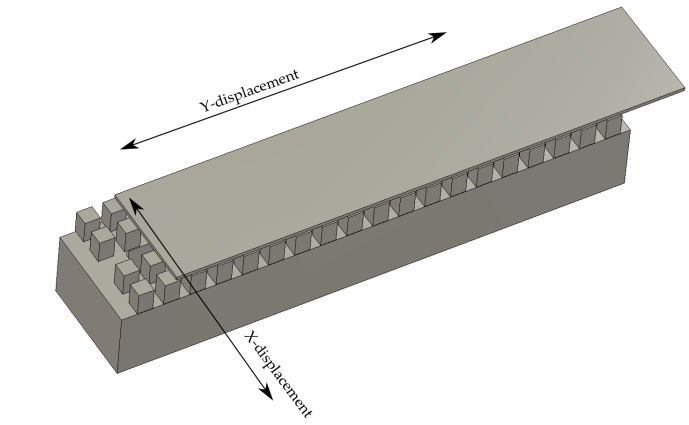

Figure 4.47: X- and Y-displacement (highly exaggerated) of the lid and matching wedge.

The simulation results for displacing the lid and wedge in x-direction by ± 50 μm is shown in Figure 4.48.

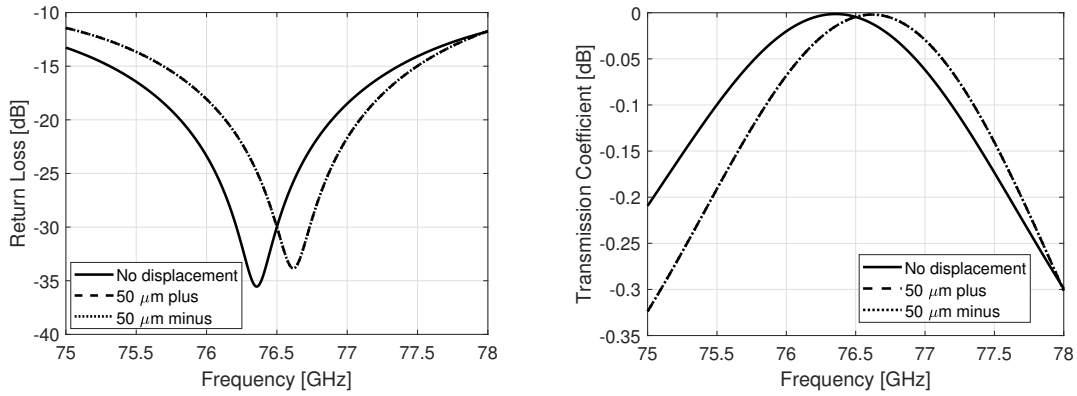

(a) Return Loss **(b)** Transmission coefficient

Figure 4.48: X-displacement effect on the (a) return loss and (b) transmission coefficient.

In Figure 4.49, the simulation results from displacing the lid and wedge in y-direction is presented. As can be seen in Figures 4.48-4.49, the displacement is causing a shift in frequency for both return loss and transmission coefficient regardless of displacement direction.

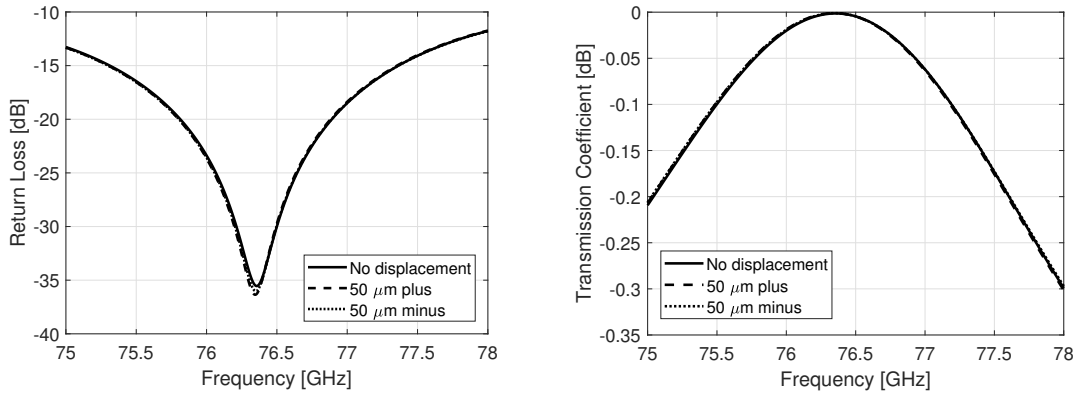

(a) Return Loss **(b)** Transmission coefficient

Figure 4.49: Y-displacement effect on the (a) return loss and (b) transmission coefficient.

5
Discussion

This chapter is separated into two main sections, adressing the two parts of this thesis work.

5.1 Part 1: Gap Waveguide Automotive Radar Antenna and Transition

The discussion for Part 1 is separated between Antenna Design and Transition Tolerance Analysis.

5.1.1 Antenna Design

In general the goals set for the single column slot antenna was more or less met, even though performance could always be further optimized. It could be a good idea to lower the ridge height by 50 μm, since an increase in distance between the ridge and slot layer would make the antenna less sensitive to manufacturing and production errors. A thinner slot layer could also be examined as to see how this can increase the performance, but from a manufacturing point-of-view it is more desireable with a larger thickness since it makes it more robust during assembly.
The single column slot antenna performs well in comparison with the microstrip reference antenna. The input matching is almost 10 dB better for the slot array over the whole frequency range, and the azimuth beam width is 25° higher for the slot antenna. The main lobe gain and elevation beam widths of the antennas are comparable, even if the side lobe level of the microstrip is approximately 1.5 dB better compared to the slot antenna. This could be further optimized by reducing the phase error which means adjusting the slot offsets from the centerline, or increasing the width of the slot layer itself. It is good to notice that the microstrip reference antenna is end-fed whereas the slot antenna is center fed, and it would be preferable to have a center-fed microstrip antenna to compare with instead.
A comparison of other antenna columns in the same frequency range as this work is shown in Table 5.1. It is seen from the table that this work performs better in certain areas such as azimuth beam width and input matching, while needing adjustment in other areas. Further optimization is possible, but there may be trade-offs. It is thus important to design the antenna for a specific automotive radar purpose; an antenna with wider azimuth beam width will detect objects at wider angles, but may have a lower main lobe gain and thus a reduced range capability.

Table 5.1: Comparison of this antenna work with already existing solutions.

Parameter	**This Work**	**Reference Antenna**	[31]	[32]
Antenna type	8-element Slot	8-element Microstrip	10-element Microstrip	4-element Hybrid Thin Film
Frequency [GHz]	76-77	76-77	77	77-81
S11 at center freq. [dB]	-25 (76.5 GHz)	-9.7 (76.5 GHz)	-15 (77 GHz)	-20 (79 GHz)
3 dB Elevation Beamwidth [deg]	10.2	11	approx. 14	49
3 dB Azimuth Beamwidth [deg]	106.2	80	approx. 70	43
Main lobe gain [dBi]	14.4	14.7	approx. 16	11
Elevation SLL [dB]	-19.2	-20.7	approx. -19	at least -20

When placing the antenna in a frame for manufacturing, the input matching is degraded by almost 8 dB for certain frequencies. It would be a possibility to further optimize the antenna with frame to lower S11 and obtain better far field performance, and then manufacture both the frame-optimized antenna and the antenna not optimized for the frame to compare their performance. The influence of a wider lid and ground plane is clearly seen on the elevation far field pattern in Figure 4.15a, since the back lobe is greatly reduced compared to the antenna without frame.

5.1.1.1 Comparison of Slot and Microstrip Arrays

The simulation results from all channels for both the slot and the microstrip array are presented in Appendix A. In Figures A.1a-A.1f, the input matching is presented for all channels. It can be seen that the slot array (bold line) is in all cases lower compared to the microstrip array channels, and this is to be expected since the microstrip will have higher losses due to the prescence of substrate. Compared to the single column antenna the matching is not heavily affected when the columns are placed in the array, but some individual column optimization could improve the matching.
The coupling between antenna columns are shown in Figures A.2a-A.2f. It is clear that the coupling between the slot columns are larger compared to the coupling between the microstrip columns, except for a small frequency span for Tx 2 and Tx

3. One of the possibilities to reduce the coupling would be to introduce corrugations between columns.
In Figures A.3a-A.3f, the azimuth far field gain is showed. In general the microstrip channels exhibits a smoother far field pattern compared to when the slot antenna is positioned in the array. The slot array exhibits larger beam width in all cases compared to the microstrip columns, but side lobe levels are lower for the microstrip case.
The elevation far field gain is shown in Figures A.4a-A.4f for all columns. In general, the side lobe levels for the slot array columns increased compared to the single column antenna, which could be due to interference and coupling between adjacent channels. This could be reduced by e.g. optimizing the slot offsets for each of the columns individually, since in the current state they do not differ between the columns. The side lobe levels are also higher for the edge elements Tx 1 and Rx 3, which could be solved by increasing the size of the slot layer.

5.1.2 Transition Tolerance Analysis

The mushrooms are the main contributor to good transition performance, as can be seen for all S-parameters. In Figure 4.19, the S11 and S22-performance is clearly highly influenced by several dB when the mushrooms are entirely removed but the pins are kept. The pins are not influencing the port matching as much, since the matching is still below -14 dB for 76-77 GHz when the pins are removed. For the transmission coefficient (S21), the pins are even causing the performance to decrease with almost 1 dB for 77 GHz.
In general, it seems as if the pins are not as sensitive to changes compared to the mushroom structure. This is shown in Figures B.1-B.2. There is a small influence on S22 for an increase in pin size, which may be due to port 2 being located so close to the pins.
The effect is far greater when changing the size by $\pm 20\mu$m of different mushroom parameters. Changing the distance from the center waveguide patch to the mushroom patch edge is not of great influence, and it is important to keep this parameter insensitive to such changes since the PCB-manufacturing might not be so accurate. A larger distance between the patch and the mushroom patch would generally introduce lower sensitivity to production errors. Both the diameter of the via hole, the mushroom patch width and the mushroom period are all parameters which seem quite sensitive to a $\pm 20\mu$m-change, as can be seen in Figures B.4-B.6. A smaller via hole diameter would gives a worse performance, just as a larger distance between the mushrooms or a larger mushroom patch width.
Changing the distance of the waveguide above the PCB will influence the result, as shown in Figure B.7. A larger distance between the PCB and the waveguide (i.e. "Plus" in the figures corresponding to an increase in parameter value) results in better port matching and transmission coefficient, but it is the smaller distance that affects the performance the most.
One of the strongest influences on the overall performance is the assembling of the lid (pins and waveguide) with the PCB. The effect of misplacing the lid by $\pm 20\mu$m is shown in Figures B.8-B.9, where it can be seen that even if the largest performance

degradation occurs for displacement in x-direction misalignments in the y-direction is almost as critical. It is therefore considered to be very important to produce a transition that will be able to tolerate these type of misalignments without ruining the performance.
In general, it is necessary to create a transition which is less sensitive to mushroom parameter errors. One of the contributors to these type of errors may be the small distances between e.g. mushroom patch-to-mushroom patch or mushroom patch-to-waveguide patch. If the mushroom patch separation is 100 μm a change of 20μm will correspond to 20% of the total length, but for larger separations a 20μm change will most likely not be as destructive. It may however be that the overall performance will be better for smaller distances, which is why a sweet-spot of small distances versus small sensitivity is desired.

5.2 Part 2: Advanced Radar Solutions

When comparing the gap waveguide to the microstrip transmission line, there are several things to discuss. It can be seen from Figure 4.21a that the microstrip line has a very flat input reflection response compared to the gap waveguide, but both are quite well-matched. What differs more is the loss shown in Figure 4.21b, where the microstrip line clearly will give more loss compared to the gap waveguide. As the length of the microstrip transmission line increases, the losses will become more substantial which in an advanced routing system could result in large losses for all transmission lines. It is also worth to note that the substrate used is a high-frequency substrate, and if cheaper substrates such as FR4 is used it may further increase the losses.
The mitering of corners is crucial in order for high performance gap waveguide routing, as can be seen from the simulation results. The possibility to make 90 degree-bends is very needed, since many high performance radar PCBs may be very crowded.
Coupling between adjacent waveguides is difficult to avoid, but is greatly reduced when two rows of pins are used. It is however very much desired to be able to use one row of pins between waveguides, at least for short distances in the routing system. Further examination of how to reduce the coupling between lines is needed, but as for all other results regarding the routing the crucial parameter seems to be the air gap between the pins and the lid. Keeping the air gap at 10 μm or less seems to be one of the keys for the routing to perform. This is not only true for the coupling between straight transmission lines, but for the overall performance as can be seen in the test structure design results in Section 4.2.2.2.
Three different gap waveguide transitions were presented in this work; two which have a smaller waveguide size with tapering to WR12 (Type I and II) and one using the standardized WR12-size without any tapering (Type III). Type II and III also had their pins aligned with the waveguide edges, whereas Type I were simply cut from a bed of pins. A comparison of their capabilities are given in Table 5.2.

Table 5.2: Comparison of routing types developed in this thesis work.

Routing Type	**Advantages**	**Disadvantages**
Type I	Manufacturing advantage since pins don't need to be tilted to follow the waveguide, Small waveguide size, Lower coupling, low transmission coefficient	Needs Tapering, Narrowband even with 2-step tapering
Type II	Smaller size, Low transmission coefficient	Pins need alignment with waveguide which can cause manufacturing difficulty, Needs tapering, Narrowband even with 2-step tapering
Type III	No taper needed giving a smaller total height, Not as narrowband, High througput	Pins need alignment with waveguide, Larger waveguide size

The main advantage of using smaller waveguide sizes is to be able to have transmission lines close together without taking up as much space. But the tapering seems to be needed in these cases, which is a large drawback both for manufacturing and also for the total height of the system. The taper may be possible to get rid of through optimization, since the bandwidth is only 1 GHz. The optimum routing waveguide would be one that have a size which is as small as possible but still as close to the WR12-size so it will not need any tapering, but this optimum might not exist.
It is also important to improve the overall return loss of the routing ports, regardless of type. There are many parts that will be connected in a radar system, and it is important to try and lower the return loss of all individual parts before merging all parts and optimizing the whole system. A return loss of -30 dB or better would be desired, but is not yet achieved. This may be performed by changing the matching wedge or adding a block as in [33].
The tolerance analysis conducted shows that displacement in xy-direction by ± 50 μm shifts both the return loss and througput up in frequency. The ± 50 μm displacement can be seen as a realistic assembly tolerance, and is therefore to be expected. No tolerance analysis were performed in z-direction, since the air gap change-simulations can be considered to stand as tolerane analysis in this case. Even though there is a small shift in performance when changing the placement of the wedge, displacement in z-direction and thus a change in air gap is much more critical to the performance of the system.

6
Conclusion

The thesis work have examined the possibility to use gap waveguide technology in automotive antennas for the W-band at 76-77 GHz. A single column 8-slot antenna have been designed and compared to a microstrip patch antenna and with existing solution. The results show that the slot antenna can compete with current solutions in terms of performance, and that the antenna array shows promise but needs further optimization in order to reach full potential.
The transition tolerance analysis shows that there are several sensitive parameters in the PCB, and that it is necessary to take this into account when designing.
The gap waveguide routing shows promise, but is yet fully finished. There is a high need for lower input reflection, whilst also allowing for larger air gap between pins and lid. When the gap waveguide routing is perfected, the losses in larger automotive radar routing systems will be greatly reduced compared to the PCB-based existing solutions today.

6.1 Future Work

There are several ideas that could be explored further, if time would not be limited.

6.1.1 Optimization of Antenna Array

It was out of the scope of this master thesis work to optimize the full antenna array to obtain better performance, since there was simply no time to do so. It would have been desired to investigate better matching, lower sidelobes and also how to reduce the coupling between columns in close proximity to one another.

6.1.2 Polarization

Many automotive systems today utilizes 45°-polarization since this can be regarded as less prone to interference. Due to no existing standard as to which direction the polarization is tilted, the interference for this type of polarization may become more common. It could also be an option to analyze how circularly polarized antenna arrays can be used in the automotive industry, and if this would give any advantages compared to linear polarizations.

6.1.3 Extension to 77-81 GHz

More and more automotive radars emerging into the market utilizes the larger bandwidth available at 77-81 GHz. The main reason for this is not only the large bandwidth, but also the higher allowed transmit power which results in desired qualities such as long range and high distance separability [5]. Extending the frequency range up to 81 GHz would require some changes in the current designs, especially for the antenna structure.

6.1.4 Waveguide-to-Antenna Transition

As of today, there is no existing transition from the gap waveguide developed in Part 2 to a double ridge waveguide to the antenna. This is an essential part in order for the whole radar system to be operational when performing the routing with gap waveguide structures.

6.1.5 Optimization of Antenna combined with Transition

It is necessary to perform optimization of the antenna and transition put together, since the merging of these two structures most likely will change the performance in terms of e.g. matching. This optimization would give a more clear idea of how the system would work if produced and implemented into a real radar system.

6.1.6 Further Routing Input Matching

A better input matching for the routing is desired, and it may be an idea to check other possibilities such as matching steps or blocks (see [33]) for the groove gap waveguide. It is also needed with a tolerance analysis for the routing, especially with the matching wedge used in the lid above each waveguide port.

Bibliography

[1] Statistics Sweden's switchboard, "Vehicles kilometres for Swedish road vehicles". Acquired 2018-03-27 from http://www.scb.se/tk1009-en.

[2] Carnegie Mellon University, "Navlab: The Carnegie Mellon University Navigation Laboratory". Acquired 2018-03-27 from http://www.cs.cmu.edu/afs/cs/project/alv/www/index.html#.

[3] Daimler Global Media Site, " The PROMETHEUS project launched in 1986: Pioneering autonomous driving". Acquired 2018-03-27 from http://media.daimler.com/marsMediaSite/en/instance/ko/The-PROMETHEUS-project-launched-in-1986-Pioneering-autonomous-driving.xhtml?oid=13744534.

[4] Society of Automotive Engineers International, "Levels of Automation". Acquired 2018-03-27 from https://autoalliance.org/wp-content/uploads/2017/07/Automated-Vehicles-Levels-of-Automation.pdf.

[5] J. Hasch, E. Topak, R. Schnabel, T. Zwick, R. Weigel, C. Waldschmidt, "Millimeter-Wave Technology for Automotive Radar Sensors in the 77 GHz Frequency Band", *IEEE Transactions on Microwave Theory and Techniques*, vol. 60, no. 3, pp. 845-860, March 2012.

[6] W. Menzel, A. Moebius, "Antenna Concepts for Millimeter-Wave Automotive Radar Sensors", *Proceedings of the IEEE*, Vol. 100, No. 7, pp. 2372-2379, July 2012.

[7] D. Pozar, "Microwave Engineering", 4th edition, Wiley 2012.

[8] Z. N. Cheng et. al, "Handbook of Antenna Technologies", Springer Science and Business Media Singapore, Vol. 2, 2016, Part IV, pp. 1389-1414.

[9] P-S. Kildal, "Foundations of Antenna Engineering", Kildal Antenn AB, Sweden: 2015.

[10] A. F. Stevenson, (1948) "Theory of slots in rectangular waveguides", *Journal of Applied Physics,* no. 19, 24–38, March 1947.

[11] S. Silver et. al, "Microwave Antenna Theory and Design", P. Peregrinus on behalf of the Institution of Electrical Engineers, Vol. 19, 1984, ch. 9, pp. 257-334.

[12] M. A. Richards, J. A. Scheer, W. A. Holm, "Introduction and Radar Overview" in Principles of Modern Radar Vol. 1, 2010, ch. 1, pp. 3-56.

[13] M. A. Richards, J. A. Scheer, W. A. Holm, "Fundamentals of Pulse Compression Waveforms" in Principles of Modern Radar Vol. 1, 2010, ch. 20, pp. 773-833.

[14] E. Hecht, "Optics", 4th ed. New York: Addison Wesley, 2001.

[15] CST Microwave Studio Home Page. http://www.cst.com/products/cstmws, Acquired 2018-06-04.

[16] T. Weiland, "Electromagnetic simulators - status and future directions," *Iet Science Measurement and Technology*, vol. 11, (6), pp. 681-686, 2017.

[17] CST Microwave Studio Home Page: Global Optimizers. `https://www.cst.com/products/csts2/optimization/global-optimizer`. Acquired 2018-06-07.

[18] P-S. Kildal, "Artificially Soft and Hard Surfaces in Electromagnetics", *IEEE Transactions on Antennas and Propagation*, vol. 38, no. 10, pp. 1537-1544, Oct. 1990. Downloaded from `http://ieeexplore.ieee.org/document/59765/`, 2018-01-15.

[19] P-S. Kildal, "Definition of artificially soft and hard surfaces for electromagnetic waves," *Electronics Letters*, vol. 24, (3), pp. 168, 1988.

[20] E. Pucci, A. U. Zaman, E. Rajo-Iglesias and P. S. Kildal, "New low loss inverted microstrip line using gap waveguide technology for slot antenna applications," Proceedings of the 5th European Conference on Antennas and Propagation (EUCAP), Rome, 2011, pp. 979-982.

[21] E. Rajo-Iglesias, P-S. Kildal, "Numerical studies of bandwidth of parallel-plate cut-off realised by a bed of nails, corrugations and mushroom-type electromagnetic bandgap for use in gap waveguides", *IET Microwaves, Antennas & Propagation*, vol. 5, no. 3, pp. 282-289, 2011. Downloaded from `http://publications.lib.chalmers.se/publication/138299`, 2018-01-15.

[22] A. Uz Zaman, V. Vassilev, P. S. Kildal and A. Kishk, "Increasing parallel plate stop-band in gap waveguides using inverted pyramid-shaped nails for slot array application above 60GHz," Proceedings of the 5th European Conference on Antennas and Propagation (EUCAP), Rome, 2011, pp. 2254-2257.

[23] A. U. Zaman, V. Vassilev, P. S. Kildal and H. Zirath, "Millimeter Wave E-Plane Transition From Waveguide to Microstrip Line With Large Substrate Size Related to MMIC Integration," in IEEE Microwave and Wireless Components Letters, vol. 26, no. 7, pp. 481-483, July 2016.

[24] E. Alfonso, A. U. Zaman, E. Pucci and P. S. Kildal, "Gap waveguide components for millimetre-wave systems: Couplers, filters, antennas, MMIC packaging," 2012 International Symposium on Antennas and Propagation (ISAP), Nagoys, 2012, pp. 243-246.

[25] M. Rezaee, A. U. Zaman and P. S. Kildal, "V-band groove gap waveguide diplexer," 2015 9th European Conference on Antennas and Propagation (EuCAP), Lisbon, 2015, pp. 1-4.

[26] A. Valero-Nogueira et al, "Planar slot-array antenna fed by an oversized quasi-TEM waveguide," *Microwave and Optical Technology Letters*, vol. 49, (8), pp. 1875-1877, 2007.

[27] P-S. Kildal, A.U. Zaman, "GAP Waveguides" in *Handbook of Antenna Technologies*, Z.N. Chen et al., Singapore: Springer Singapore, 2016, vol. 4, part VII, pp. 3247-3347. Downloaded from `http://publications.lib.chalmers.se/publication/253896-gap-waveguides`, 2018-01-15.

[28] A. Jimenez Saez et al, "Single-Layer Cavity-Backed Slot Array Fed by Groove Gap Waveguide," *IEEE Antennas and Wireless Propagation Letters*, vol. 15, pp. 1402-1405, 2016.

[29] D. Zarifi et al, "Design and Fabrication of a High-Gain 60-GHz Corrugated Slot Antenna Array With Ridge Gap Waveguide Distribution Layer," *IEEE Transactions on Antennas and Propagation*, vol. 64, (7), pp. 2905-2913, 2016.

[30] Rogers Corporation, "RT/duroid 6202 High Frequency Laminates Data Sheet". 2017. Aquired 2018-05-22 from `https://www.rogerscorp.com/documents/610/acs/RT-duroid-6202-Laminate-Data-Sheet.pdf`.

[31] J. Xu et.al, "An Array Antenna for Both Long- and Medium-Range 77 GHz Automotive Radar Applications", *IEEE Transactions on Antennas and Propagation*, Vol. 65, no. 12, pp. 7207-7216, dec. 2017.

[32] O Khan et.al, "Hybrid Thin Film Antenna for Automotive Radar at 79 GHz", *IEEE Transactions on Antennas and Propagation*, Vol. 65, no. 10, pp. 5076-5085, Oct. 2017.

[33] A. Farahbakhsh, D. Zarifi and A. U. Zaman, "60-GHz Groove Gap Waveguide Based Wideband H-Plane Power Dividers and Transitions: For Use in High-Gain Slot Array Antenna", *IEEE Transactions on Microwave Theory and Techniques*, Vol. 65 pp. 4111-4121, 2017.

A

Appendix 1: Antenna Array Comparison

A.1 Antenna Array Comparison

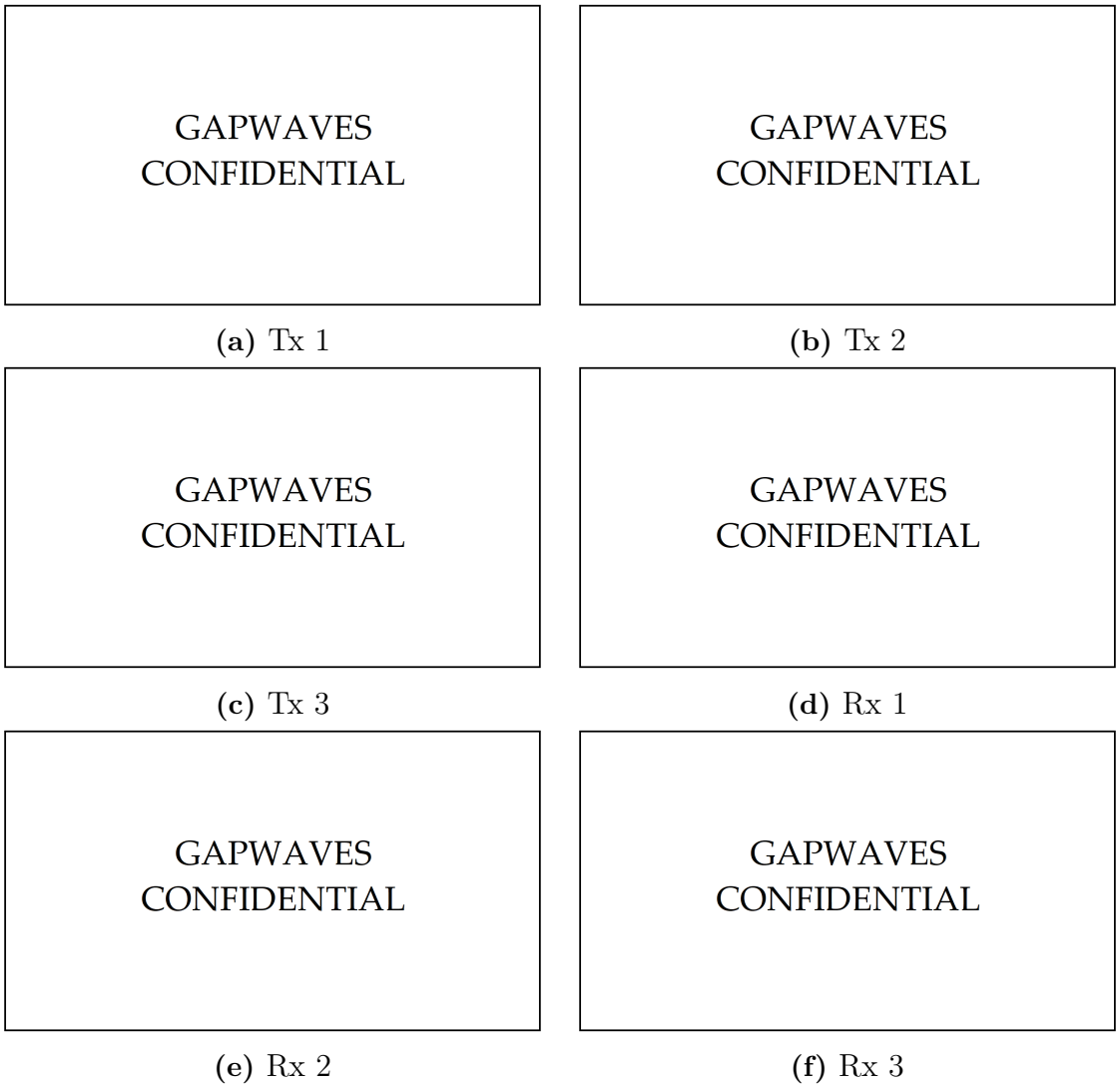

(a) Tx 1 **(b)** Tx 2

(c) Tx 3 **(d)** Rx 1

(e) Rx 2 **(f)** Rx 3

Figure A.1: Input matching for all ports for both the slot and the microstrip array antenna.

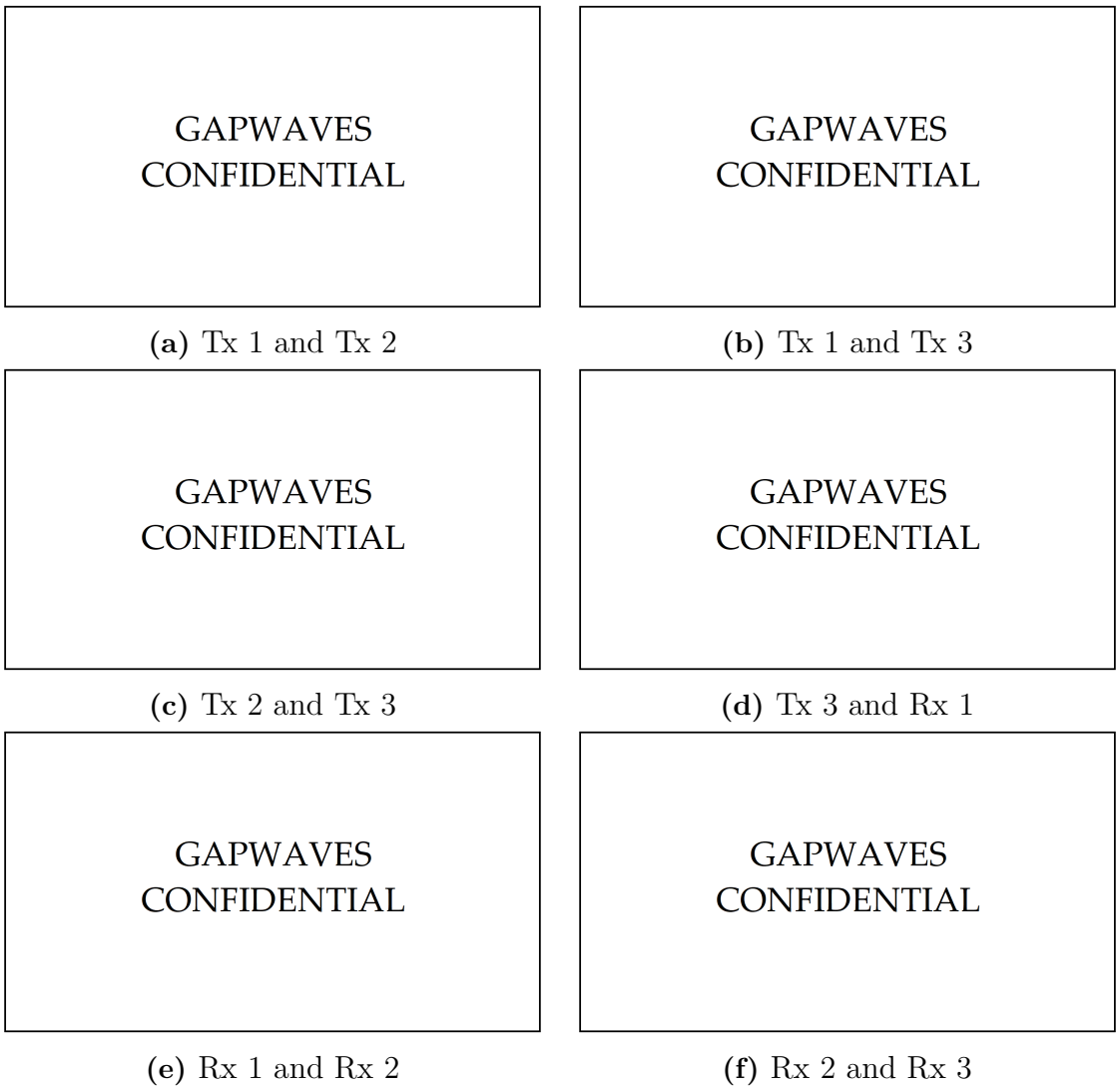

(a) Tx 1 and Tx 2

(b) Tx 1 and Tx 3

(c) Tx 2 and Tx 3

(d) Tx 3 and Rx 1

(e) Rx 1 and Rx 2

(f) Rx 2 and Rx 3

Figure A.2: Coupling for both the slot and the microstrip array antenna.

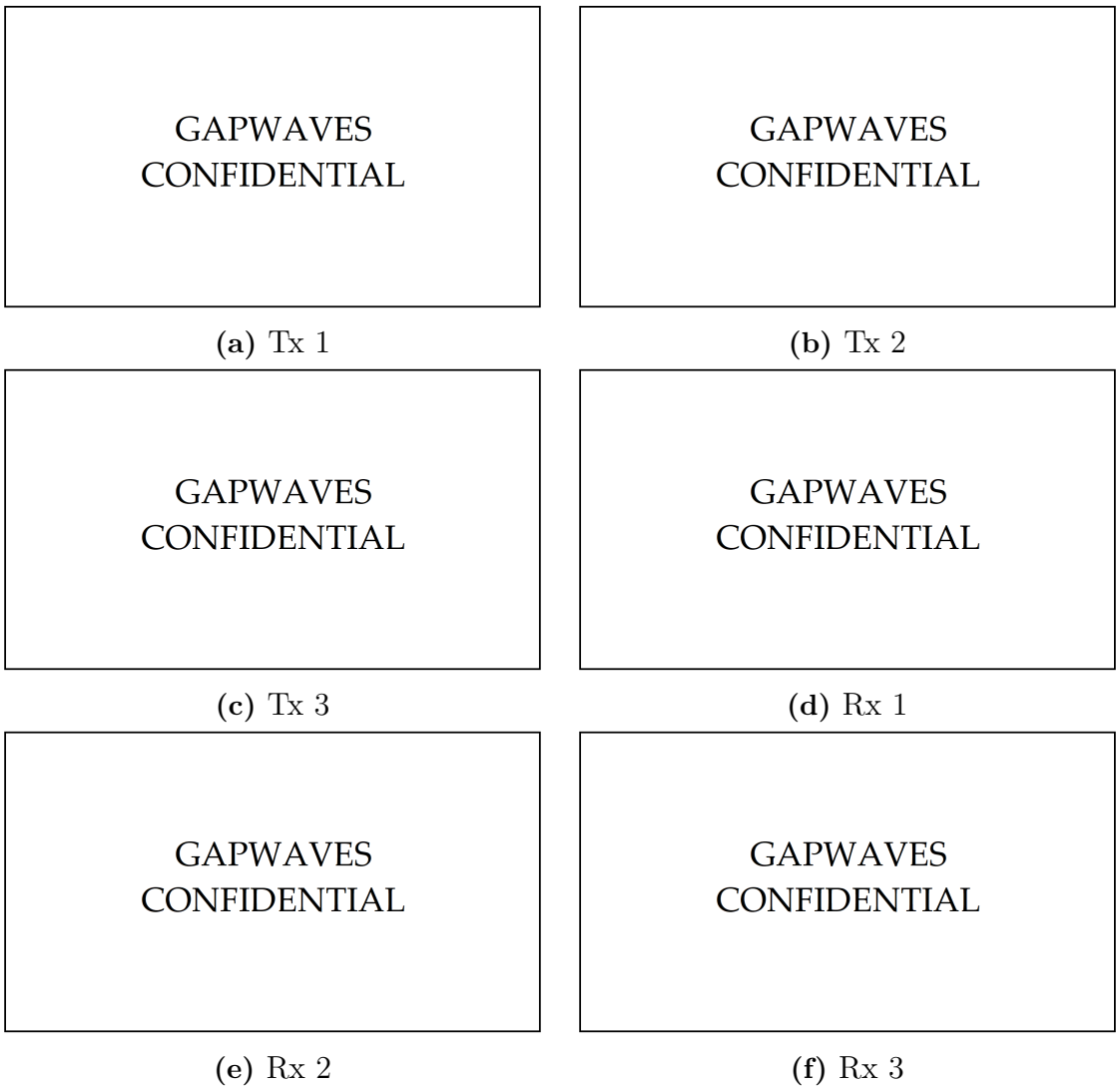

(a) Tx 1 **(b)** Tx 2

(c) Tx 3 **(d)** Rx 1

(e) Rx 2 **(f)** Rx 3

Figure A.3: Azimuth far field gain for all antennas, for both the slot and the microstrip array.

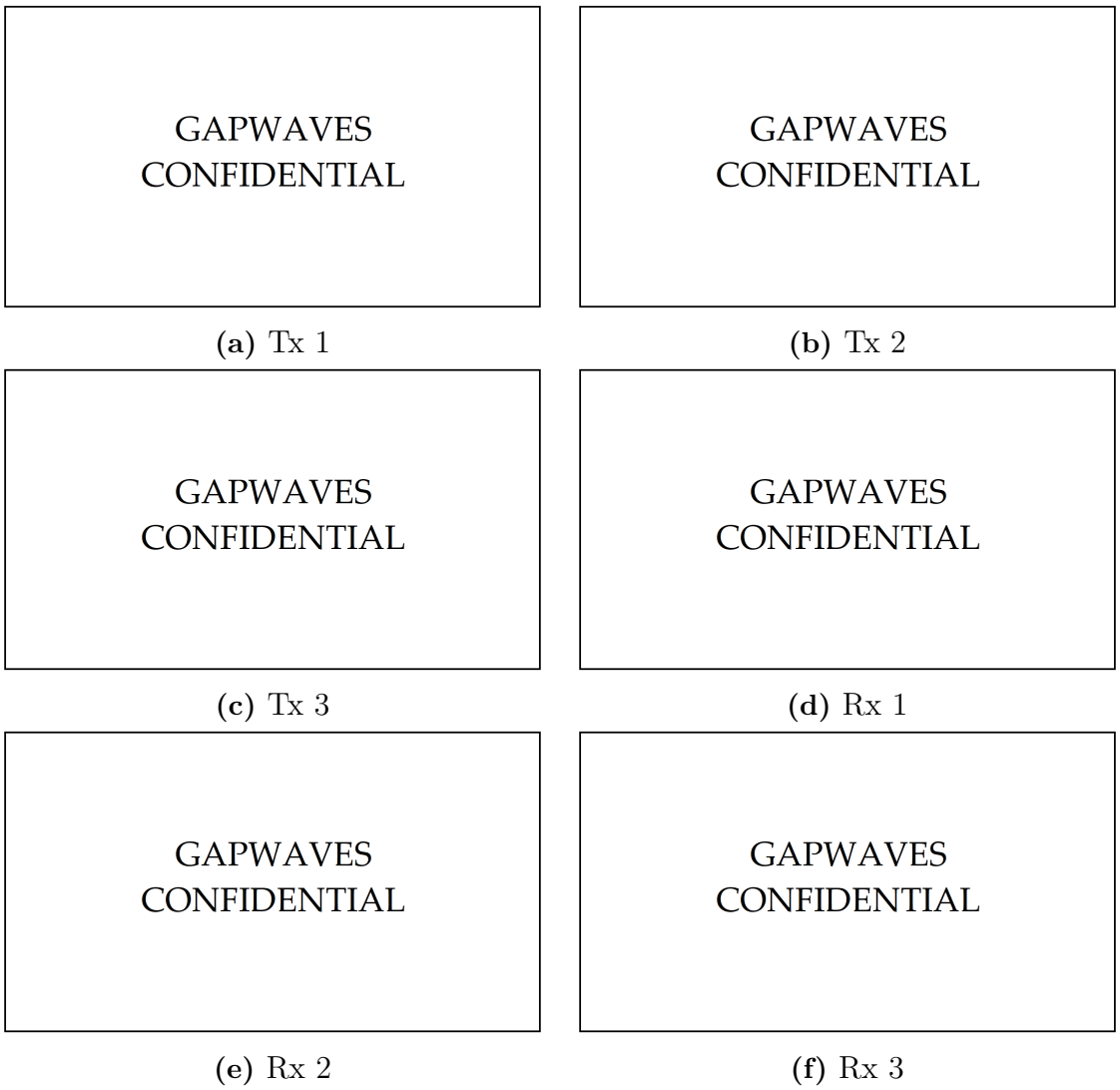

(a) Tx 1 **(b)** Tx 2

(c) Tx 3 **(d)** Rx 1

(e) Rx 2 **(f)** Rx 3

Figure A.4: Elevation far field gain for all antennas, for both the slot and the microstrip array.

B

Appendix 2: Transition Tolerance Analysis

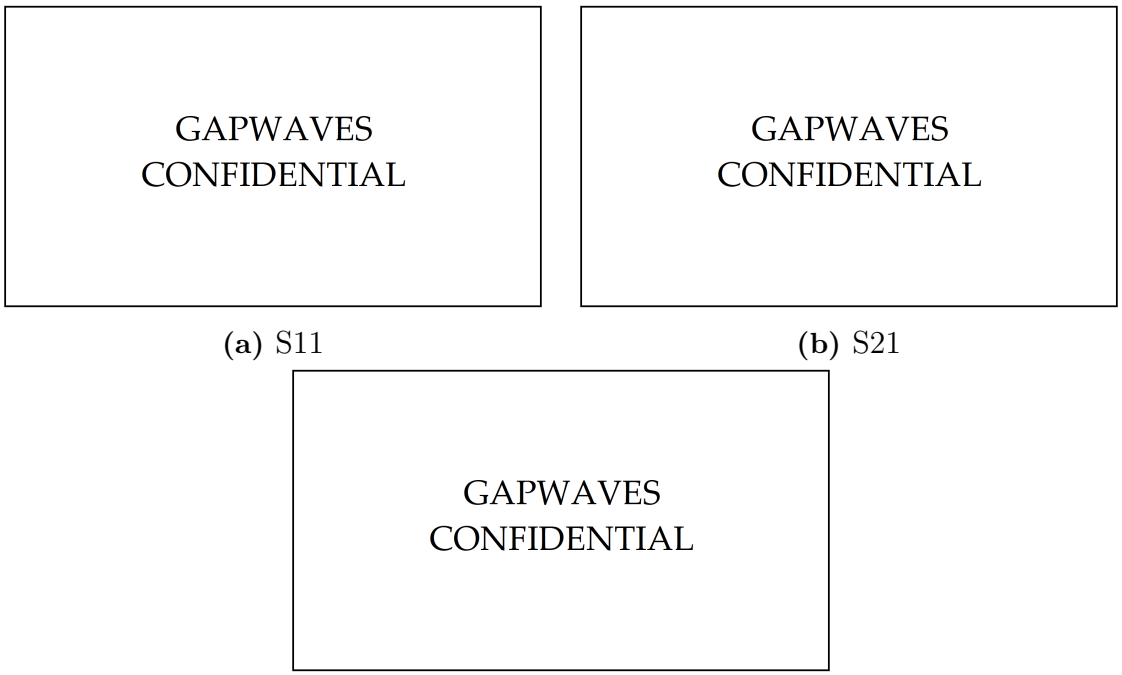

(a) S11 **(b)** S21

(c) S22

Figure B.1: PinLineH

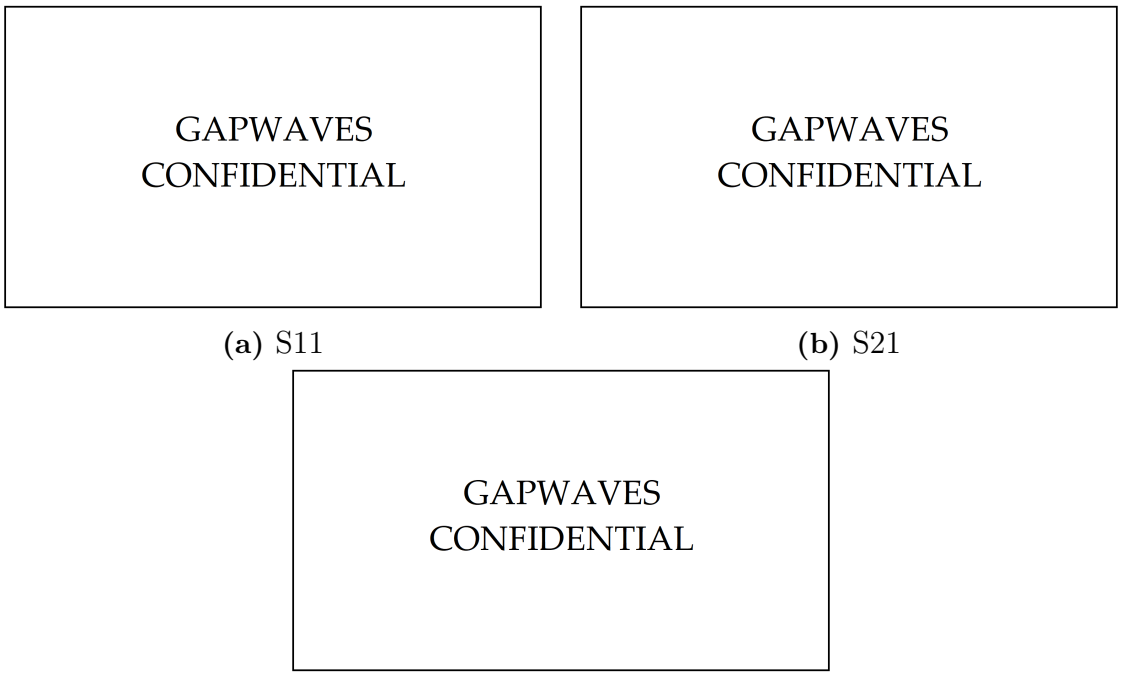

(a) S11 **(b)** S21

(c) S22

Figure B.2: PinWidth

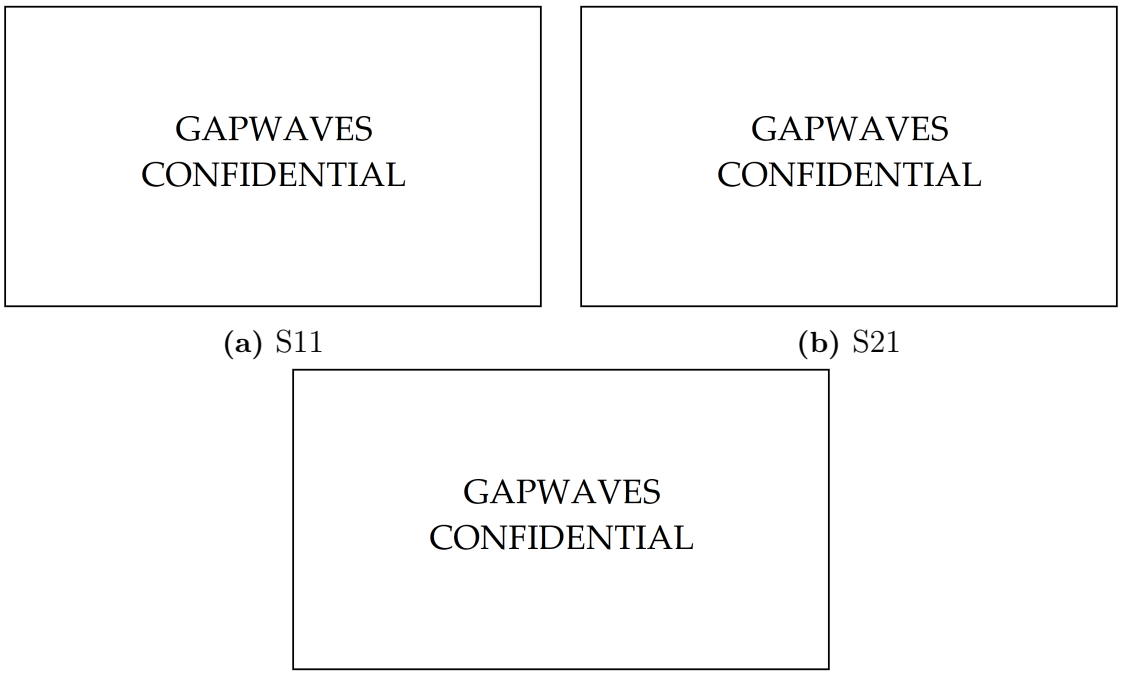

(a) S11 **(b)** S21

(c) S22

Figure B.3: Distance from patch to mushroom

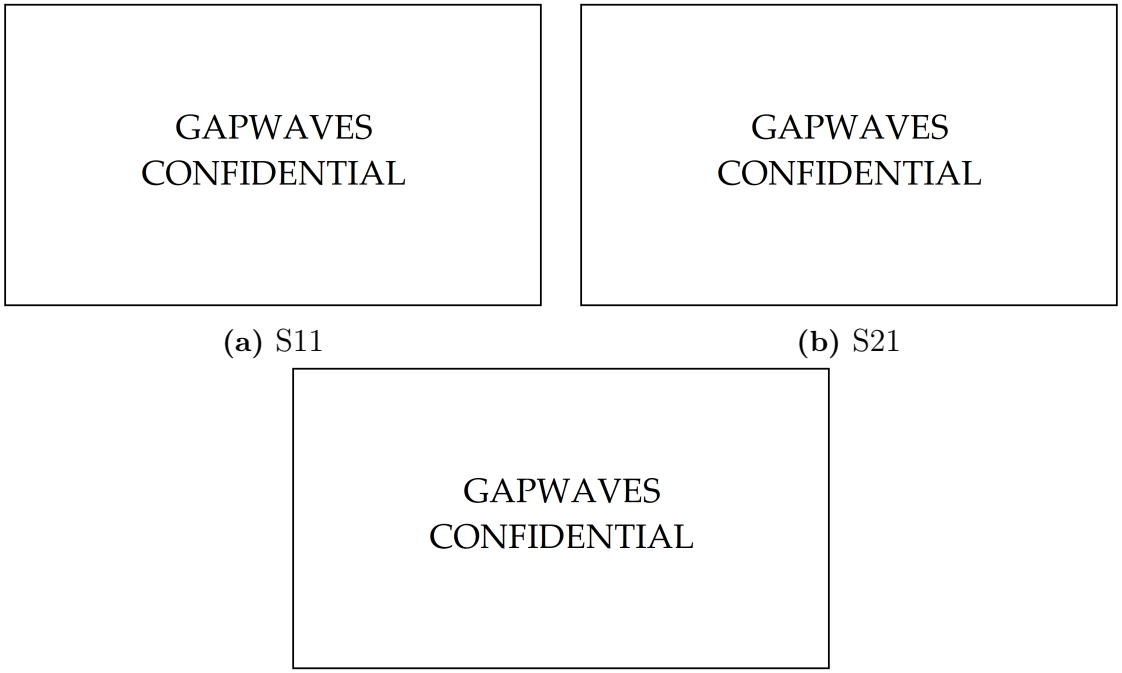

(a) S11 **(b)** S21

(c) S22

Figure B.4: Via hole diameter

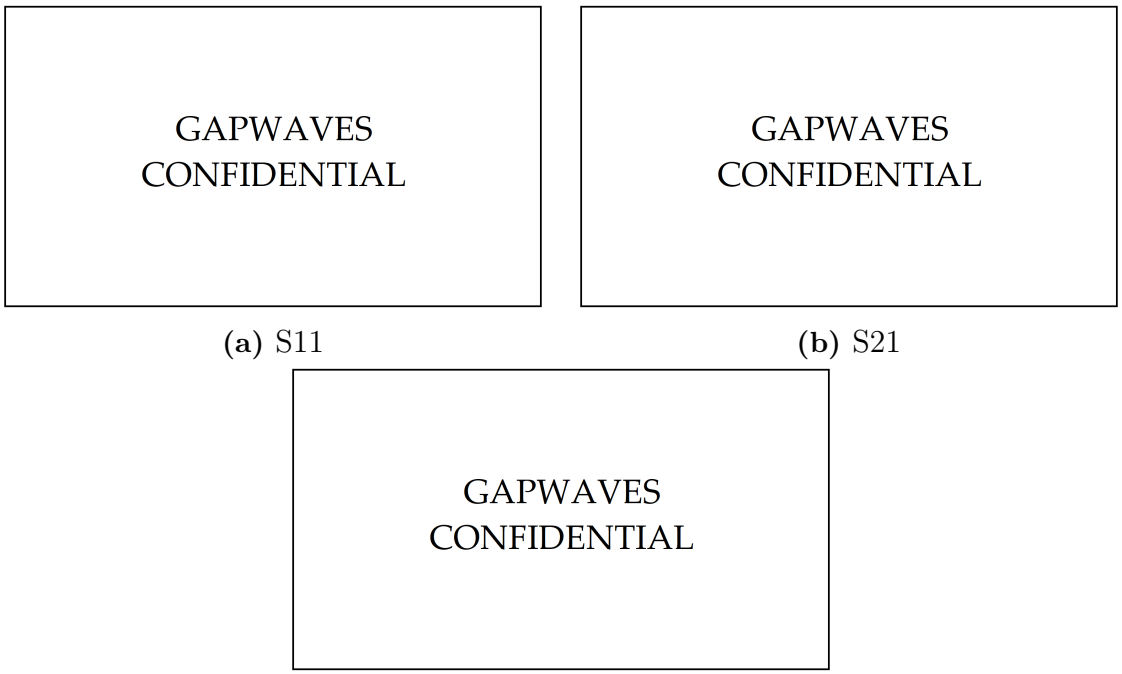

(a) S11 **(b)** S21

(c) S22

Figure B.5: Mushroom period

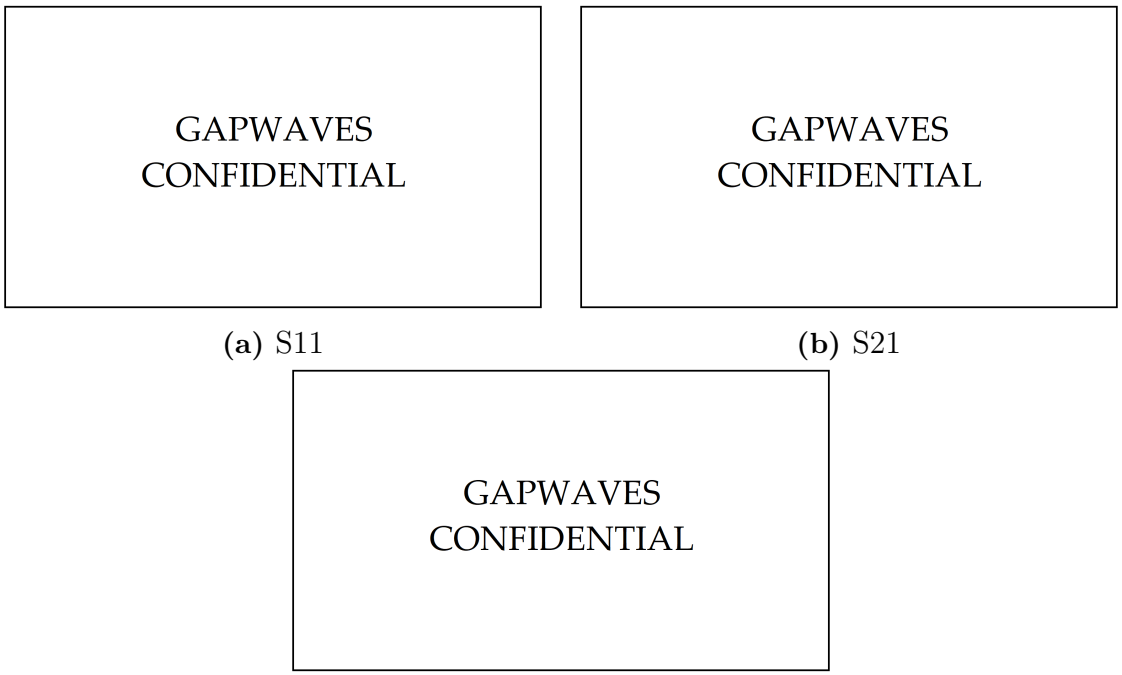

(a) S11 **(b)** S21

(c) S22

Figure B.6: Mushroom patch width

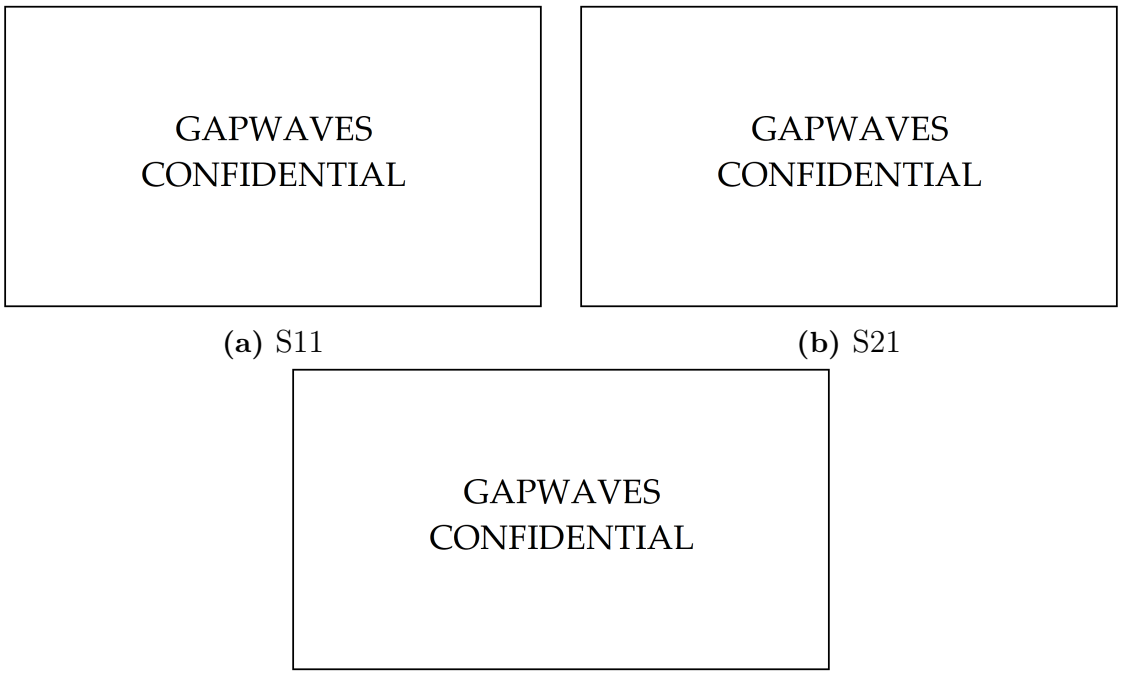

(a) S11 **(b)** S21

(c) S22

Figure B.7: Distance between PCB and waveguide

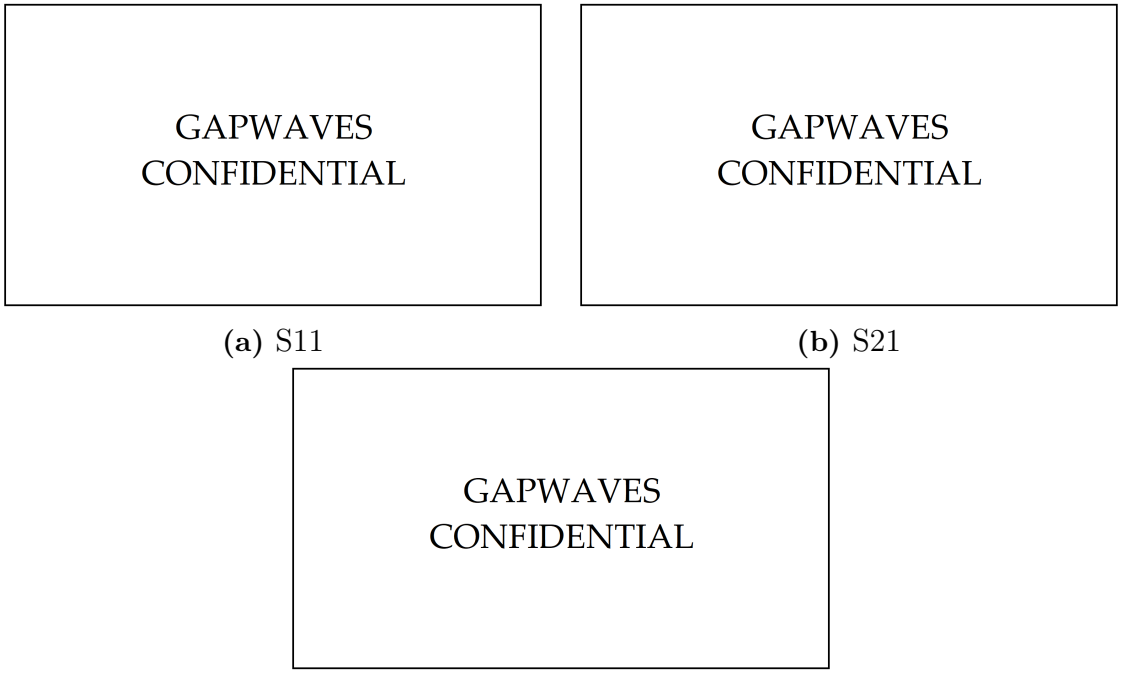

(a) S11 **(b)** S21

(c) S22

Figure B.8: Displacement of lid and pins in X-direction

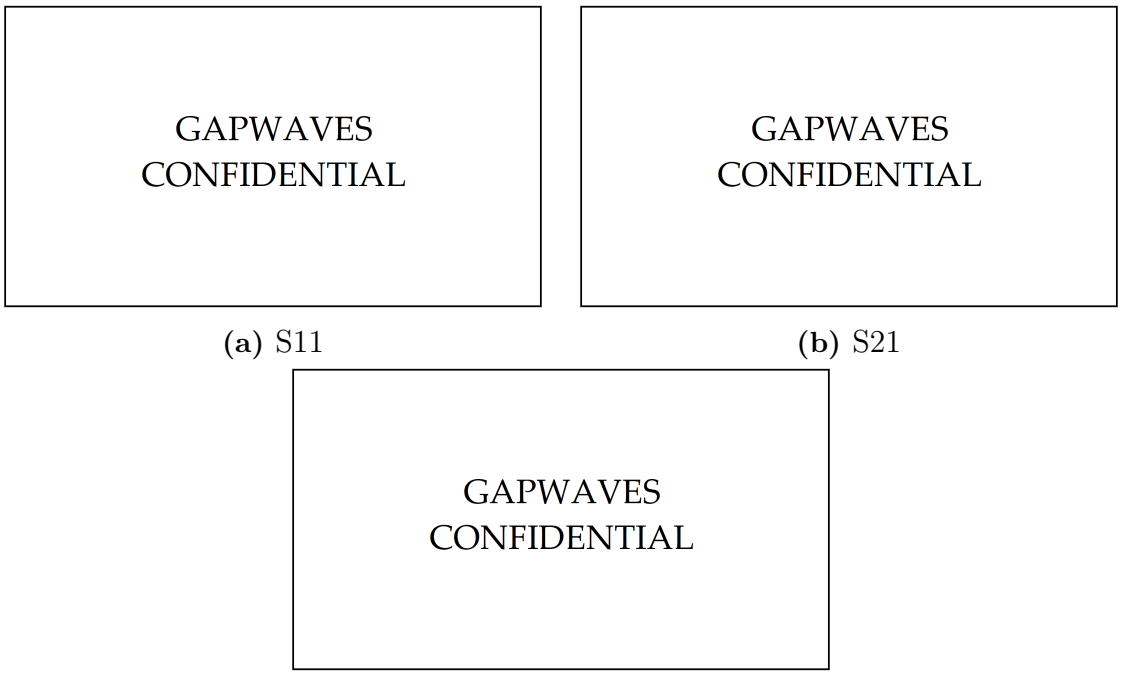

(a) S11 **(b)** S21

(c) S22

Figure B.9: Displacement of lid and pins in Y-direction